Inorg. Chem. **2004**, *43*, 6979–6994

Spectroscopic Properties and Electronic Structure of Pentammineruthenium(II) Dinitrogen Oxide and Corresponding Nitrosyl Complexes: Binding Mode of N_2O and Reactivity

Florian Paulat, Torben Kuschel, Christian Näther, V. K. K. Praneeth, Ole Sander, and Nicolai Lehnert*

Institut für Anorganische Chemie, Christian-Albrechts-Universität Kiel, Olshausenstrasse 40, D-24098 Kiel, Germany

Received May 28, 2004

The spectroscopic properties and the electronic structure of the only nitrous oxide complex existing in isolated form, $[Ru(NH_3)_5(N_2O)]X_2$ (**1**, X = Br^-, BF_4^-), are investigated in detail in comparison to the nitric oxide precursor, $[Ru(NH_3)_5(NO)]X_3$ (**2**). IR and Raman spectra of **1** and of the corresponding ^{15}NNO labeled complex are presented and assigned with the help of normal coordinate analysis (NCA) and density functional (DFT) calculations. This allows for the identification of the Ru–N_2O stretch at ~300 cm^{-1} and for the unambiguous definition of the binding mode of the N_2O ligand as N-terminal. Obtained force constants are 17.3, 9.6, and 1.4 mdyn/Å for N–N, N–O, and Ru–N_2O, respectively. The Ru(II)–N_2O bond is dominated by π back-donation, which, however, is weak compared to the NO complex. This bond is further weakened by Coulomb repulsion between the fully occupied t_{2g} shell of Ru(II) and the HOMO of N_2O. Hence, nitrous oxide is an extremely weak ligand to Ru(II). Calculated free energies and formation constants for $[Ru(NH_3)_5(L)]^{2+}$ (L = NNO, N_2, OH_2) are in good agreement with experiment. The observed intense absorption at 238 nm of **1** is assigned to the $t_{2g} \rightarrow \pi^*$ charge transfer transition. These data are compared in detail to the spectroscopic and electronic structural properties of NO complex **2**. Finally, the transition metal centered reaction of nitrous oxide to N_2 and H_2O is investigated. Nitrous oxide is activated by back-donation. Initial protonation leads to a weakening of the N–O bond and triggers electron transfer from the metal to the NN–OH ligand through the π system. The implications of this mechanism for biological nitrous oxide reduction are discussed.

Introduction

Despite the biological and environmental significance of nitrous oxide, not much is known about the coordination chemistry of this molecule. In fact, only one transition metal complex of N_2O has been prepared and isolated so far, and the coordination mode of the nitrous oxide ligand in this system is still a matter of discussion. This compound, $[Ru(NH_3)_5(N_2O)]$ X_2 (**1**), is a Ru(II) complex with pentammine coligands. Attempts to isolate other transition metal N_2O complexes have mostly yielded metal oxide, nitride, or nitrosyl products so far.[1] Complex **1** was first reported as an unstable species in solution.[2] Later, it was also possible to isolate **1** as a solid with different counterions X (X = Cl^-, Br^-, BF_4^-, etc.).[3−5] IR data have been reported for **1**, and a simple normal coordinate analysis was performed to explore whether these vibrational data are consistent with end-on N or O coordination of the N_2O ligand. It was found that O coordination is in better agreement with the experimental data.[3] This was later challenged, and it was claimed

* Corresponding author. E-mail: nlehnert@ac.uni-kiel.de.

10.1021/ic049302i CCC: $27.50
Published on Web 10/02/2004

(1) (a) Yamamoto, A.; Kitazume, S.; Pu, L. S.; Ikeda, S. *J. Am. Chem. Soc.* **1971**, *93*, 371−380. (b) Bottomley, F.; Lin, I. J. B.; Mukaida, M. *J. Am. Chem. Soc.* **1980**, *102*, 5238−5242. (c) Bottomley, F.; Paez, D. E.; White, P. S. *J. Am. Chem. Soc.* **1982**, *104*, 5651−5657. (d) Bottomley, F. *Polyhedron* **1992**, *11*, 1707−1731. (e) Vaughan, G. A.; Sofield, C. D.; Hillhouse, G. L.; Rheingold, A. L. *J. Am. Chem. Soc.* **1989**, *111*, 5491. (f) Matsunaga, P. T.; Hillhouse, G. L.; Rheingold, A. L. *J. Am. Chem. Soc.* **1993**, *115*, 2075. (g) Smith, M. R., III; Matsunaga, P. T.; Anderson, R. A. *J. Am. Chem. Soc.* **1993**, *115*, 7049. (h) Koo, K.; Hillhouse, G. L.; Rheingold, A. L. *Organometallics* **1995**, *14*, 456. (i) Groves, J. T.; Roman, J. S. *J. Am. Chem. Soc.* **1995**, *117*, 5594−5595. (j) Laplaza, C. E.; Odom, A. L.; Davis, W. M.; Cummins, C. C.; Protasiewicz, J. D. *J. Am. Chem. Soc.* **1995**, *117*, 4999−5000. (k) Johnson, A. R.; Davis, W. M.; Cummins, C. C.; Serron, S.; Nolan, S. P.; Musaev, D. G.; Morokuma, K. *J. Am. Chem. Soc.* **1998**, *120*, 2071−2085. (l) Khoroshun, D. V.; Musaev, D. G.; Morokuma, K. *Organometallics* **1999**, *18*, 5653−5660. (m) Cherry, J.-P. F.; Johnson, A. R.; Baraldo, L. M.; Tsai, Y.-C.; Cummins, C. C.; Kryatov, S. V.; Rybak-Akimova, E. V.; Capps, K. B.; Hoff, C. D.; Haar, C. M.; Nolan, S. P. *J. Am. Chem. Soc.* **2001**, *123*, 7271−7286. (n) Kaplan, A. W.; Bergman, R. G. *Organometallics* **1997**, *16*, 1106−1108. (o) McCarthy, M. R.; Crevier, T. J.; Bennett, B.; Dehestani, A.; Mayer, J. M. *J. Am. Chem. Soc.* **2000**, *122*, 12391−12392.

that nitrous oxide is coordinated with its terminal N atom based on mechanistic data[4] and NMR results for a related system.[6] Although experimental evidence is in favor of N coordination of N_2O, it is surprising that this point has never been clarified in the literature. Since there is no crystal structure available for **1**, the most promising approach to define the bonding mode of N_2O is the complete assignment of the metal−ligand stretching vibrations of **1** in connection with a normal coordinate analysis. However, the Ru(II)−N_2O stretching vibration has not been identified so far. The UV absorption spectrum of **1** shows an intense transition at 238 nm which, however, has not been assigned yet. It was noted that N_2O is a weak ligand, but the nature of the Ru(II)−N_2O bond has not been defined. Hence, although complex **1** has been known for quite some time, neither the spectroscopic properties nor the electronic structure of this complex nor the properties of N_2O as a ligand itself have been explored in detail so far.

Recently, the coordination chemistry of nitrous oxide has gained considerable interest due to its biological significance. The enzyme nitrous oxide reductase (N2OR) catalyses the final step in denitrification, i.e., the reduction of N_2O to N_2 following the equation[7]

$$N_2O + 2H^+ + e^- \rightarrow N_2 + H_2O \qquad (1)$$

The catalytically active center of N2OR (called Cu_Z) is a cluster of four copper ions which are bridged by a central sulfide.[8−10] The resting state of the enzyme has been characterized by a number of spectroscopic methods,[11] which ultimately lead to the assignment of one Cu(II) and three Cu(I) for resting Cu_Z.[12] Reduction of this cluster by one electron leads to the catalytically active state with four Cu(I) which is EPR silent.[13] The binding of nitrous oxide to the reduced Cu_Z cluster was evaluated using density functional (DFT) calculations.[13] It was found that N_2O can bind to the cluster in various geometries; i.e., it is coordinated either end-on with its terminal N atom to Cu_I (resting Cu_Z) or side-on bridging between Cu_I and Cu_{IV} (reduced Cu_Z). In the calculations, this bridging mode leads to an increased transfer of electron density to N_2O which would be favorable for its reduction and protonation.

Besides the interest in N_2O reduction and protonation originating from bioinorganic chemistry, this process is also of great importance from an environmental point of view. Because of the increased use of nitrate containing fertilizers in agriculture, a large amount of nitrous oxide is produced by denitrifying bacteria living in soil and seawater and subsequently released to the atmosphere.[14] In addition, burning of fossil fuels contributes to the N_2O emission.[15] This way, nitrous oxide has become the third most important green house gas. Hence, the properties of nitrous oxide and its reactivity are not only of interest for bioinorganic chemistry, but also of global importance. Although the reduction of N_2O to dinitrogen and water (eq 1) is highly exothermic ($\Delta G^\circ \approx -80$ kcal/mol), this gas is metastable and unreactive due to a kinetic barrier to its decomposition.

In this study, the spectroscopic properties and the electronic structure of the complex $[Ru(NH_3)_5(N_2O)]X_2$ (**1**) using bromide (**1-Br**) and tetrafluoroborate (**1-BF_4**) counterions are investigated. Raman spectra of nitrous oxide complexes are presented for the first time. Using ^{15}N isotope substitution, the IR and Raman spectra of **1** are fully assigned including Ru−N_2O stretching and bending vibrations using a quantum-chemistry assisted normal coordinate analysis (QCA-NCA).[16] In comparison to DFT calculations on both N and O coordinated isomers of **1**, this allows for an unambiguous definition of the coordination mode of the N_2O ligand. From these calculations, the electronic structure of complex **1** is also investigated, and the properties of nitrous oxide as a ligand are evaluated. Time-dependent DFT calculations are used to assign the UV−vis spectrum of **1**. The free energy

(2) (a) Armor, J. N.; Taube, H. *J. Am. Chem. Soc.* **1969**, *91*, 6874−6876. (b) Armor, J. N.; Taube, H. *J. Am. Chem. Soc.* **1970**, *92*, 2560−2562. (c) Armor, J. N.; Taube, H. *J. Am. Chem. Soc.* **1971**, *93*, 6476.

(3) (a) Diamantis, A. A.; Sparrow, G. J. *Chem. Commun.* **1970**, 819−820. (b) Diamantis, A. A.; Sparrow, G. J. *J. Colloid Interface Sci.* **1974**, *47*, 455−458. (c) Diamantis, A. A.; Sparrow, G. J.; Snow, M. R.; Norman, T. R. *Aust. J. Chem.* **1975**, *28*, 1231−1244.

(4) Bottomley, F.; Brooks, W. V. F. *Inorg. Chem.* **1977**, *16*, 501−502.

(5) (a) Bottomley, F.; Crawford, J. R. *Chem. Commun.* **1971**, 200−201. (b) Bottomley, F.; Crawford, J. R. *J. Am. Chem. Soc.* **1972**, *94*, 9092−9095. (c) Bottomley, F.; Brooks, W. V. F.; Clarkson, S. G.; Tong, S.-B. *Chem. Commun.* **1973**, 919−920. (d) Bottomley, F.; Clarkson, S. G.; Tong, S.-B. *J. Chem. Soc., Dalton Trans.* **1974**, 2344−2346. (e) Bottomley, F. *Acc. Chem. Res.* **1978**, *11*, 158−163. (f) Wolfe, S. K.; Andrade, C.; Swinehart, J. H. *Inorg. Chem.* **1974**, *13*, 2567−2572.

(6) Pamplin, C. B.; Ma, E. S. F.; Safari, N.; Rettig, S. J.; James, B. R. *J. Am. Chem. Soc.* **2001**, *123*, 8596−8597.

(7) (a) Ferguson, S. J. *Curr. Opin. Chem. Biol.* **1998**, *2*, 182−193. (b) Richardson, D. J.; Watmough, N. J. *Curr. Opin. Chem. Biol.* **1999**, *3*, 207−219. (c) Moura, I.; Moura, J. J. G. *Curr. Opin. Chem. Biol.* **2001**, *5*, 168−175.

(8) Brown, K.; Tegoni, M.; Prudêncio, M.; Pereira, A. S.; Besson, S.; Moura, J. J. G.; Moura, I.; Cambillau, C. *Nat. Struct. Biol.* **2000**, *7*, 191.

(9) (a) Rasmussen, T.; Berks, B. C.; Sanders-Loehr, J.; Dooley, D. M.; Zumft, W. G.; Thomson, A. J. *Biochemistry* **2000**, *39*, 12753−12756. (b) Alvarez, M. L.; Ai, J.; Zumft, W. G.; Sanders-Loehr, J.; Dooley, D. M. *J. Am. Chem. Soc.* **2001**, *123*, 576−587.

(10) (a) Brown, K.; Djinovic-Carugo, K.; Haltia, T.; Cabrito, I.; Saraste, M.; Moura, J. J. G.; Moura, I.; Tegoni, M.; Cambillau, C. *J. Biol. Chem.* **2000**, *275*, 41133−41136. (b) Haltia, T.; Brown, K.; Tegoni, M.; Cambillau, C.; Saraste, M.; Mattila, K.; Djinovic-Carugo, K. *Biochem. J.* **2003**, *369*, 77−88.

(11) (a) Farrar, J. A.; Thomson, A. J.; Cheesman, M. R.; Dooley, D. M.; Zumft, W. G. *FEBS Lett.* **1991**, *294*, 11. (b) Neese, F.; Ph.D. Thesis, Universität Konstanz, Germany, 1996. (c) Farrar, J. A.; Zumft, W. G.; Thomson, A. J. *Proc. Natl. Acad. Sci. U.S.A.* **1998**, *95*, 9891. (d) Prudêncio, M.; Pereira, A. S.; Tavares, P.; Besson, S.; Cabrito, I.; Brown, K.; Samyn, B.; Devreese, B.; VanBeeumen, J.; Rusnak, F.; Fauque, G.; Moura, J. J. G.; Tegoni, M.; Cambillau, C.; Moura, I. *Biochemistry* **2000**, *39*, 3899.

(12) (a) Chen, P.; DeBeer George, S.; Cabrito, I.; Antholine, W. E.; Moura, J. J. G.; Moura, I.; Hedman, B.; Hodgson, K. O.; Solomon, E. I. *J. Am. Chem. Soc.* **2002**, *124*, 744−745. (b) Chen, P.; Cabrito, I.; Moura, J. J. G.; Moura, I.; Solomon, E. I. *J. Am. Chem. Soc.* **2002**, *124*, 10497−10507.

(13) Ghosh, S.; Gorelsky, S. I.; Chen, P.; Cabrito, I.; Moura, J. J. G.; Moura, I.; Solomon, E. I. *J. Am. Chem. Soc.* **2003**, *125*, 15708−15709.

(14) (a) Intergovernmental Panel on Climate Change (IPCC). *The Science of Climate Change*; Cambridge University Press: New York, 1995. (b) Battle, M. *Nature* **1996**, *383*, 231−235. (c) Kroeze, C.; Mosier, A.; Bouwman, L. *Global Biogeochem. Cycles* **1999**, *13*, 1−8. (d) Bange, H. W. *Nature* **2000**, *408*, 301−302. (e) Robertson, G. P.; Paul, E. A.; Harwood, R. R. *Science* **2000**, *289*, 1922−1925.

(15) (a) Berges, M. G. M.; Hofman, R. M.; Scharffe, D.; Crutzen, P. J. *J. Geophys. Res.* **1993**, *98*, 18527. (b) Becker, K. H.; Lörzer, J. C.; Kurtenbach, R.; Wiesen, P. *Environ. Sci. Technol.* **1999**, *33*, 4134−4139.

(16) Lehnert, N.; Tuczek, F. *Inorg. Chem.* **1999**, *38*, 1659−1670.

for ligand binding is calculated for **1** in comparison to related compounds. Finally, the reduction and protonation of end-on terminally coordinated N_2O are investigated.

Ru−NO complexes with various coligands have drawn considerable interest recently due to their significance as antitumor and antiseptic agents.[17] In this study, the Ru(II)−NO^+ precursor complex $[Ru(NH_3)_5(NO)]X_3$ (**2**) using bromide (**2-Br**), tetrafluoroborate (**2-BF$_4$**), and triflate (**2-OTf**) counterions has also been investigated in comparison with **1**. Although **2** has been the topic of numerous studies, it is quite surprising that the spectroscopic assignments for this complex are incomplete. Vibrational spectra are presented for **2** together with force constants obtained from normal coordinate analysis using QCA-NCA. The results show that complex **2** exchanges its nitrosyl oxygen during synthesis. For **2-Br**, an unusual splitting of the N−O stretching vibration is observed which is explained on the basis of the crystal structure of **2-Br** presented here. The electronic structure of **2** is briefly discussed, and the electronic spectra are assigned. The mechanistic implications of the observed oxygen exchange of NO during the synthesis are discussed. These data obtained for complex **2** serve as a reference for a quantitative interpretation of the results for **1**.

Experimental and Computational Procedures

Syntheses. Reactions were performed using Schlenk techniques. The starting material $RuCl_3$ was purchased from Aldrich. The precursor complexes $[Ru(NH_3)_5(Cl)]Cl_2$ and $[Ru(NH_3)_6]Cl_3$ were prepared according to literature procedures.[18] NO gas was passed through a potassium hydroxide column and then through a cold trap at −80 °C prior to usage to remove higher nitrogen oxide impurities.

$[Ru(NH_3)_5(NO)]Br_3$ (2-Br). This complex can be prepared by two different methods. (a) Following a procedure of Armor et al.,[19] 0.3 g of $[Ru(NH_3)_6]Cl_3$ is dissolved in 35 mL of degassed 0.1 M hydrobromic acid, and then, NO is passed through the solution for about 25 min. The solution changes its color from yellow to orange. The solution is then reduced to half of its volume and stored in the refrigerator. After a few days, orange crystals of $[Ru(NH_3)_5(NO)]X_3$ (X = Cl, Br) have formed. The crystals are collected by filtration and washed with 3 M HBr, ethanol, and water. Yield: 75%. To obtain pure **2-Br**, the raw product is recrystallized several times from 1 M HBr. (b) Following a method by Gleu et al.,[20] 0.4 g of $[Ru(NH_3)_5(Cl)]Cl_2$ is dissolved in ∼12 mL of water and heated until boiling. The solution is removed from the oil bath, and 12 mL of concentrated NH_3 solution is added to the hot solution. Then, 1.2 g of $(NH_4)(S_2O_8)$ is added slowly, and the solution is swirled. A pale yellow precipitate of $[Ru(NH_3)_5(NO)](SO_4)_{1/2}(S_2O_8)_{1/2}$ forms immediately which is collected by filtration after about 1 h. The product is washed with 2 M NH_3 solution and acetone and dried. Yield: 25%.

The obtained raw product is then refluxed with concentrated HCl for about 15 min to obtain $[Ru(NH_3)_5(NO)]Cl_3$ (**2-Cl**) in high yield (95%). Repeated recrystallization from 1 M HBr yields **2-Br**. Structural data are available in Table 1.

Table 1. Crystal Data and Results of the Structure Refinement for Compound **2-Br**

chemical formula	$[Ru(NH_3)_5NO]Br_3 \cdot H_2O$
fw	474.0
T	room temperature
λ	0.71073
cryst syst	orthorhombic
space group	*Pnma*
a	12.234(1)
b	6.9982(4)
c	14.479(1)
V	1246.9(1)
Z	4
D_{calcd}	2.444
μ	10.85
R1[a] [$I > 2\sigma(I)$]	0.0292
wR2 [all data]	0.0842

[a] $R1 = \sum||F_o| - |F_c||/\sum|F_o|$; $wR2 = [\sum[w(F_o^2 - F_c^2)^2]/\sum[w(F_o^2)^2]]^{1/2}$.

$[Ru(NH_3)_5(NO)](BF_4)_3$ (2-BF$_4$) and $[Ru(NH_3)_5(NO)](OTf_4)_3$ (2-OTf). Compound **2-BF$_4$** is insoluble in water or acid and can therefore be prepared by dissolving **2-Cl** in water and adding 1 M HBF_4. The product precipitates as yellow powder. Compound **2-OTf**, on the other hand, is very soluble in water. It is obtained by repeated recrystallization of **2-Cl** from 2.5 M CF_3SO_3H solution as yellow powder in relatively low yield.

$[Ru(NH_3)_5(N_2O)]X_2$ (1). Preparation of the nitrous oxide complex **1-Br** (X = Br) follows the procedure of Bottomley et al.[5b] Complex $[Ru(NH_3)_5(NO)]Br_3$ (112 mg) and 1.12 g of $NH_2OH \cdot HX$ (X = Cl, Br; 1:1 mixture) are dissolved in 10 mL of degassed water in an ice bath. Then, 5 pellets (about 1 g) of NaOH are added, and **1-Br** starts precipitating immediately as pale yellow solid. The reaction is stopped after 3−5 min by filtration. The obtained product is washed with oxygen-free ethanol and diethyl ether and dried in vacuo. Yield: 67%. The preparation of **1-BF$_4$** is complicated by the fact that the precursor **2-BF$_4$** is insoluble in water. Complex $[Ru(NH_3)_5(NO)](BF_4)_3$ (100 mg) and 560 mg of $NH_2OH \cdot HBF_4$ are suspended in ∼12 mL of degassed water in an ice bath. On addition of the NaOH pellets, the precursor **2-BF$_4$** starts dissolving while at the same time pale yellow **1-BF$_4$** precipitates. In order to ensure completion of the reaction, the mixture is stirred for 5 min and then filtered. Yield: 93%. The corresponding complex with triflate could not be obtained by this method, because the triflate salts are too soluble in water.

Crystal Structure Determination. The data were collected using a 4-circle diffractometer from STOE & CIE and were corrected for absorption effects. The structure was solved with direct methods using SHELXS-97 and was refined against F^2 using SHELXL-97. All non-H atoms were refined anisotropically. The H-atoms were positioned with idealized geometry and refined using the riding model. One bromide anion is disordered in two positions and was refined using a split model. The $[Ru(NH_3)_5NO]$ unit is located on a crystallographic mirror plane, and the NO ligand is disordered in two positions due to symmetry. This disorder remains constant in the noncentrosymmetric space group $Pna2_1$.

In this space group, it is not possible to decide if the two different orientations are unequally occupied or not. However, in this case

(17) (a) Chanda, N.; Mobin, S. M.; Puranik, V. G.; Datta, A.; Niemeyer, M.; Lahiri, G. K. *Inorg. Chem.* **2004**, *43*, 1056−1064. (b) Marchenko, A. V.; Vedernikov, A. N.; Dye, D. F.; Pink, M.; Zaleski, J. M.; Caulton, K. G. *Inorg. Chem.* **2004**, *43*, 351−360. (c) Patra, A. K.; Mascharak, P. K. *Inorg. Chem.* **2003**, *42*, 7363−7365. (d) Hirano, T.; Oi, T.; Nagao, H.; Morokuma, K. *Inorg. Chem.* **2003**, *42*, 6575−6583. (e) Marchenko, A. V.; Vedernikov, A. N.; Dye, D. F.; Pink, M.; Zaleski, J. M.; Caulton, K. G. *Inorg. Chem.* **2002**, *41*, 4087−4089. (f) Hadadzadeh, H.; DeRosa, M. C.; Yap, G. P. A.; Rezvani, A. R.; Crutchley, R. J. *Inorg. Chem.* **2002**, *41*, 6521−6526. (g) Nagao, H.; Hirano, T.; Tsuboya, N.; Shiota, S.; Mukaida, M.; Oi, T.; Yamasaki, M. *Inorg. Chem.* **2002**, *41*, 6267−6273.

(18) Allen, A. D.; Bottomley, F.; Harris, R. O.; Reinsalu, V. P.; Senoff, C. V. *Inorg. Synth.* **1970**, *12*, 2−8.

(19) Armor, J. N.; Scheidegger, H. A.; Taube, H. *J. Am. Chem. Soc.* **1968**, *90*, 5928−5929.

(20) Gleu, K.; Büddecker, I. *Z. Anorg. Allg. Chem.* **1952**, *268*, 202−220.

the absolute structure cannot be refined. To check if, e.g., an ordered super structure is present, one additional data set was measured at low temperatures using an IPDS from STOE & CIE. However, from these investigations there is no hint for a super structure or any change of the symmetry.

UV−Vis Spectroscopy. Absorption spectra were recorded either in KBr disks or for pure solids (between sapphire windows) at 10 K using a Varian Cary 5 UV−vis−NIR spectrometer equipped with a CTI cryocooler.

Vibrational Spectroscopy. FT-Raman spectra were recorded on a Bruker IFS 66 interferometer with a Bruker FRA 106 Raman attachment using a Nd:YAG laser for excitation ($\lambda = 1064$ nm). Measurements were performed on pure compounds. Resolution was set to 2 cm^{-1}. Middle- and far-infrared spectra (MIR & FIR) were recorded on a Bruker IFS 66v vacuum instrument at room temperature. For the MIR region, KBr disks were used, and the spectra were recorded at a resolution of 1 cm^{-1}. In the far-IR region, PE pellets were used, and the resolution was set to 2 cm^{-1}. Low-temperature MIR spectra were obtained on a Mattson Genesis type I spectrometer equipped with a cryogenic CTI cryostat. Spectra were recorded at 20 K at a resolution of 1 cm^{-1}.

Normal Coordinate Analysis. Normal coordinate calculations were performed using the QCPE computer program 576 by M. R. Peterson and D. F. McIntosh which involves solution of the secular equation $\mathbf{GFL} = \lambda\mathbf{L}$ by the diagonalization procedure of Miyazawa.[21] The calculations are based on a general valence force field; force constants are refined with the nonlinear optimization routine of the simplex algorithm according to Nelder and Mead.[22] The simplex optimization was used to refine only selected force constants according to the quantum-chemical assisted normal coordinate analysis.[16] Here, a force field from DFT calculations is used as a starting point to generate initial force constants, and a subset of these is fit to reproduce the known experimental frequencies. For the NCA, the H atoms of the NH_3 ligands have been removed since the objective is to obtain force constants for the Ru−NO and Ru−N_2O subunits. For the resulting "N" ligands, an effective mass of 18 has been used resembling NH_3. This leads to the simplified models $[Ru(N_5)(NO)]$ ($\hat{\mathbf{2}}$) and $[Ru(N_5)(N_2O)]$ ($\hat{\mathbf{1}}$) which are based on the calculated structures but which have further been symmetrized (by setting all N−Ru−N angles to 90°) to have C_{4v} symmetry.

Density Functional Calculations. Spin-restricted DFT calculations using Becke's three parameter hybrid functional with the correlation functional of Lee, Yang, and Parr (B3LYP[23]) were performed using the program package Gaussian 98.[24]The structures of the cations $[Ru(NH_3)_5(N_2O)]^{2+}$ ($\tilde{\mathbf{1}}$) and $[Ru(NH_3)_5(NO)]^{3+}$ ($\tilde{\mathbf{2}}$) were fully optimized using the LanL2DZ basis set. Calculated vibrational frequencies show that the obtained geometries represent true minima since no imaginary frequencies were found. IR and Raman intensities were calculated as well for vibrational assignments. The LanL2DZ basis set applies Dunning/Huzinaga full double-ζ (D95)[25] basis functions on first row and Los Alamos effective core potentials plus DZ functions on all other atoms.[26] For calculating the absorption spectrum of $\tilde{\mathbf{1}}$ and $\tilde{\mathbf{2}}$, the time-dependent DFT formalism as implemented in G98 has been applied. To calculate the binding constants for ligands L in $[Ru(NH_3)_5(L)]^{2+}$, the structures of the cations $[Ru(NH_3)_5]^{2+}$ and $[Ru(NH_3)_5(L)]^{2+}$ with $L = H_2O$, N_2 have been fully optimized. In addition, $[Ru(NH_3)_5]^{3+}$ has also been fully optimized. All these structures represent true minima as evident from frequency calculations. To investigate the protonation of the coordinated N_2O ligand and the subsequent splitting of the N−O bond, the structures of $[Ru(NH_3)_5(NNOH)]^{3+}$ and of $[Ru(NH_3)_5(NN)]^{4+}$ have been fully optimized as well. Solvation effects were included in the calculations of the reaction energies in Scheme 1 using the Polarized Continuum Model (PCM)[27] with water as solvent ($\epsilon = 78$). In all calculations, convergence was reached when the relative change in the density matrix between subsequent iterations was less than 1×10^{-8}. Atomic charges were calculated using the natural population analysis (NPA). Force constants in internal coordinates were extracted from the Gaussian output using the program Redong[28] (QCPE 628). Orbitals were plotted with the program GaussView.

Results and Analysis

A. Crystal Structure, Spectroscopy, and Electronic Structure of $[Ru(NH_3)_5(NO)]^{3+}$ (2). In order to explore the spectroscopic properties and the electronic structure of $[Ru(NH_3)_5(N_2O)]X_2$ (**1**), the precursor complex $[Ru(NH_3)_5(NO)]X_3$ (**2**) has been investigated first. In comparison, this allows for a quantitative evaluation of the results obtained for **1**, since the electronic structure and reactivity of complex **2** are known from a number of studies.[29−31] First, the crystal structure of $[Ru(NH_3)_5(NO)]Br_3$ is presented. Vibrational data for **2** with different counterions are assigned with the help of density functional (DFT) calculations and a normal coordinate analysis. Finally, low-temperature UV−vis spectra of **2** are assigned using time-dependent DFT (TD-DFT) calculations.

A.1. Crystal Structure. Compound **2-Br** crystallizes in the orthorhombic space group *Pnma* with 4 formula units in the unit cell. The asymmetric unit consists of one $[Ru(NH_3)_5(NO)]^{3+}$ unit, three crystallographically independent bromide anions, and one water molecule, all of them located on crystallographic mirror planes. The ruthenium cations are coordinated by 5 ammonia molecules and one NO ligand. Due to symmetry, the NO group is disordered

(21) Miyazawa, T. *J. Chem. Phys.* **1958**, *29*, 246.
(22) Nelder, J. A.; Mead, R. *Comput. J.* **1965**, *7*, 308.
(23) (a) Becke, A. D. *Phys. Rev. A* **1988**, *38*, 3098. (b) Becke, A. D. *J. Chem. Phys.* **1993**, *98*, 1372. (c) Becke, A. D. *J. Chem. Phys.* **1993**, *98*, 5648.
(24) Frisch, M. J.; Trucks, G. W.; Schlegel, H. B.; Scuseria, G. E.; Robb, M. A.; Cheeseman, J. R.; Zakrzewski, V. G.; Montgomery, J. A., Jr.; Stratmann, R. E.; Burant, J. C.; Dapprich, S.; Millam, J. M.; Daniels, A. D.; Kudin, K. N.; Strain, M. C.; Farkas, O.; Tomasi, J.; Barone, V.; Cossi, M.; Cammi, R.; Mennucci, B.; Pomelli, C.; Adamo, C.; Clifford, S.; Ochterski, J.; Petersson, G. A.; Ayala, P. Y.; Cui, Q.; Morokuma, K.; Malick, D. K.; Rabuck, A. D.; Raghavachari, K.; Foresman, J. B.; Cioslowski, J.; Ortiz, J. V.; Stefanov, B. B.; Liu, G.; Liashenko, A.; Piskorz, P.; Komaromi, I.; Gomperts, R.; Martin, R. L.; Fox, D. J.; Keith, T.; Al-Laham, M. A.; Peng, C. Y.; Nanayakkara, A.; Gonzalez, C.; Challacombe, M.; Gill, P. M. W.; Johnson, B. G.; Chen, W.; Wong, M. W.; Andres, J. L.; Head-Gordon, M.; Replogle, E. S.; Pople, J. A. *Gaussian 98*, revision A.11; Gaussian, Inc.: Pittsburgh, PA, 1998.
(25) *Modern Theoretical Chemistry*; Dunning, T. H., Jr., Hay, P. J., Schaefer, H. F., III, Eds.; Plenum: New York, 1976.
(26) (a) Hay, P. J.; Wadt, W. R. *J. Chem. Phys.* **1985**, *82*, 270, 299. (b) Wadt, W. R.; Hay, P. J. *J. Chem. Phys.* **1985**, *82*, 284.
(27) Cramer, C. J.; Truhlar, D. G. *Chem. Rev.* **1999**, *99*, 2161−2200.
(28) Allouche, A.; Pourcin, J. *Spectrochim. Acta* **1993**, *49A*, 571.
(29) (a) Enemark, J. H.; Feltham, R. D. *Coord. Chem. Rev.* **1974**, *13*, 339. (b) Bottomley, F. *Coord. Chem. Rev.* **1978**, *26*, 7−32. (c) Westcott, B. L.; Enemark, J. H. *Transition Metal Nitrosyls*; Solomon, E. I., Lever, A. B. P., Eds.; Wiley: New York, 1999; Vol. 2, p 403.
(30) Callahan, R. W.; Meyer, T. J. *Inorg. Chem.* **1977**, *16*, 574−581.
(31) Czap, A.; van Eldik, R. *J. Chem. Soc., Dalton Trans.* **2003**, 665−671.

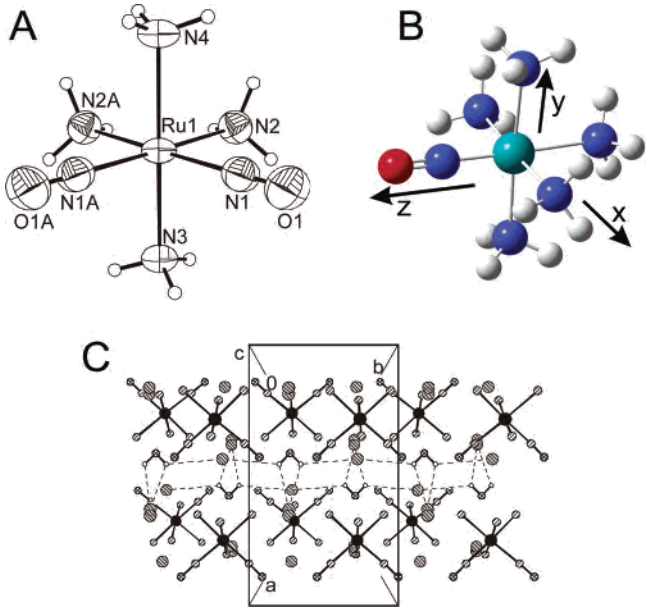

Figure 1. (A) Crystal structure of the $[Ru(NH_3)_5(NO)]^{3+}$ unit in **2-Br** with labeling. Displacement ellipsoids are drawn at the 50% probability level. The two NO groups indicate the positions of disordering. (B) Optimized structure from DFT calculations. (C) Crystal structure of compound **2-Br** with view along the crystallographic *c* axis (N-hydrogen atoms are omitted for clarity).

in two positions and superimposed with one ammonia ligand (see Experimental Section). Figure 1A shows the $[Ru(NH_3)_5(NO)]^{3+}$ cation with two NO units indicating the disordered positions. Important distances and angles are given in the Supporting Information Table 5. In the crystal structure, the $[Ru(NH_3)_5(NO)]^{3+}$ units are stacked in the direction of the crystallographic *a*-axis. The bromide ions are connected by O−H···Br hydrogen bridges via the water molecules (Figure 1C).

A.2 Vibrational Spectra and Assignment. The IR spectrum of $[Ru(NH_3)_5(NO)]Br_3$ is shown in Figure 2 including the corresponding ^{15}NO isotope labeled data. For the labeling experiments, $^{15}N^{18}O$ has been used. However, the observed shifts do only correspond to the presence of the ^{15}N in the complex (see NCA). This shows that complex **2** exchanges its nitrosyl oxygen during synthesis. Isotope sensitive bands are present at 1927/1912 and 602 cm^{-1} in **2-Br** which shift to 1889/1873 and 588 cm^{-1}, respectively, on isotope substitution. These bands are assigned to the N−O stretch and the Ru−N−O linear bend (doubly degenerate), respectively. In the corresponding Raman spectra in Figure 3, the N−O stretch is found at 1927/1911 cm^{-1} and the Ru−NO stretch at 594 cm^{-1}, respectively. These shift to 1888/1872 and 590 cm^{-1}, respectively, on ^{15}N isotope labeling. These assignments are confirmed by normal coordinate analysis (vide infra). The splitting of ν(N−O) into two bands could be due to a correlation effect in the solid state. However, this seems unlikely since the observed intensity pattern (1911, strong; 1927, weak) is identical for IR and Raman. In addition, the splitting and intensity pattern is conserved on isotope substitution, which excludes Fermi resonance. This indicates that there are two different NO molecules in the crystal with a slightly different environment, which is in accordance with the observed disorder (vide infra). These two species would then give rise to the two observed bands. Since no superstructure reflections could be found experimentally, the distribution of the NO ligands over the two positions must be random. Other bands in the IR and Raman spectra belong to the $[Ru(NH_3)_5]^{2+}$ subunit of **2-Br** and can be assigned with the help of a DFT calculation.

Calculated IR and Raman spectra for $[Ru(NH_3)_5(NO)]^{3+}$ are shown in Figures 2 and 3 in comparison with experimental results for **2-Br**. The complete assignments are summarized in Table 6 in the Supporting Information. The N−O stretch is calculated at 1905 cm^{-1} in very good agreement with experiment. In the calculations, the two Ru−N−O linear bends are calculated at ∼590 cm^{-1} and the Ru−NO stretch at 567 cm^{-1}, which resembles the experimental order of the vibrational energies. In agreement with the calculations, the linear bends are not observed in the Raman spectrum. Vice versa, the Ru−NO stretch is predicted by the calculations to be Raman active but only weakly IR active, and accordingly, this mode is not observed in the IR data for **2-Br**. Additional vibrations occurring in this spectral region are the Ru−NH_3 stretches. These modes are predicted to be Raman active only by the calculations and, hence, are assigned to the strong Raman bands at 508 and 487 cm^{-1}. The weak IR bands at 473 and 450 cm^{-1} are also identified with these vibrations.

In summary, with the help of DFT calculations the IR and Raman spectra of **2-Br** have been completely assigned. The most striking differences between the calculations and experiment occur (a) for the N−H stretching and H−N−H bending modes due to anharmonicity[32] and (b) for the metal−ligand vibrations, the energy of which is underestimated in the calculations. The assignment of the N−H stretching and bending vibrations is in agreement with work of Mercer et al.[33] However, their assignment of ν(Ru−NO) to the IR band at ∼600 cm^{-1} and of the Ru−N−O bends to a very weak band below 400 cm^{-1} is not in agreement with the isotope data and calculations presented here. In addition, their assignment of ν(Ru−NH_3) to IR bands below 500 cm^{-1} only is incomplete. Table 6 in the Supporting Information also shows the complete vibrational assignments for **2-BF_4**, which are very similar to those of **2-Br**. Importantly, in the IR spectrum of **2-BF_4** both the Ru−N−O linear bends (at 609 cm^{-1}) and the Ru−NO stretch (weak band at 589 cm^{-1}) are observed, which further supports the above assignments. Finally, Table 6 in the Supporting Information gives the vibrational assignments for **2-OTf**. Both **2-BF_4** and **2-OTf** do not show a splitting of the N−O stretch which further indicates that this splitting in the case of **2-Br** is not an

(32) All the vibrations above 1000 cm^{-1} (with exception of the N−O stretch) correspond to modes that have dominant hydrogen displacement character. Strikingly, all these vibrations are calculated up to 10% too high in energy compared to experiment (cf. Supporting Information Table 6). This deviation is due to the anharmonicity of these modes which is not taken into account by the calculations.

(33) Mercer, E. E.; McAllister, W. A.; Durig, J. R. *Inorg. Chem.* **1966**, *5*, 1881−1886.

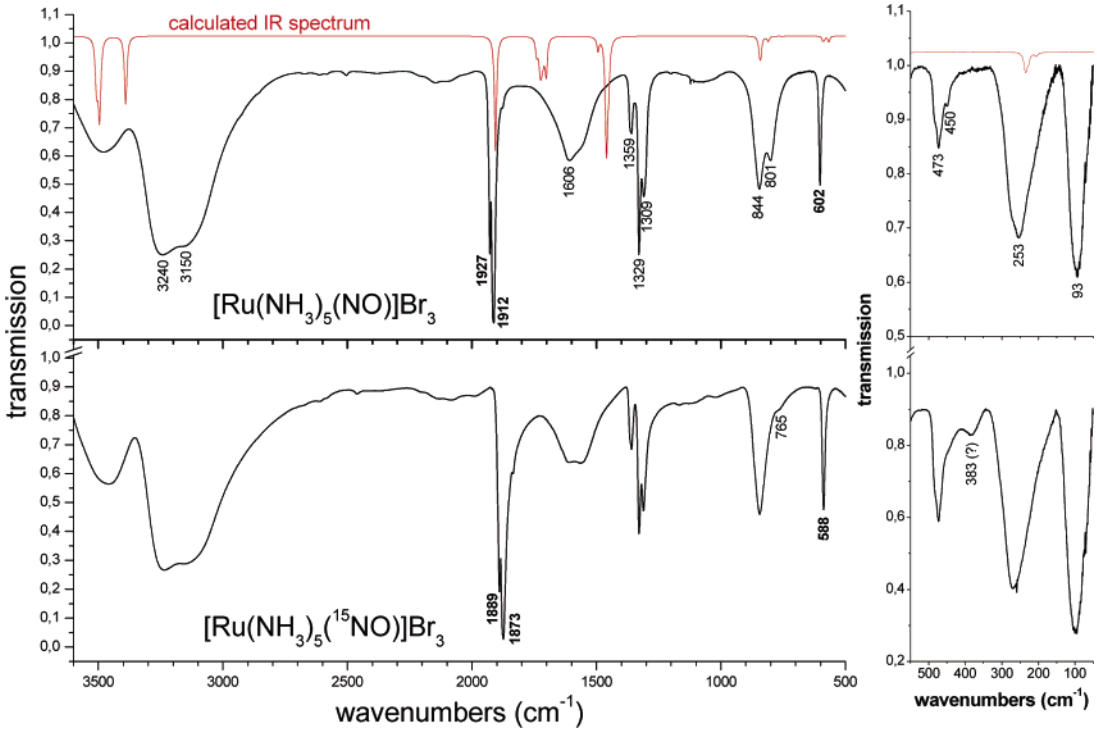

Figure 2. IR spectrum of **2-Br** (top) and of the corresponding ^{15}NO isotope labeled complex (bottom). The calculated spectrum is also included in the top panel as indicated.

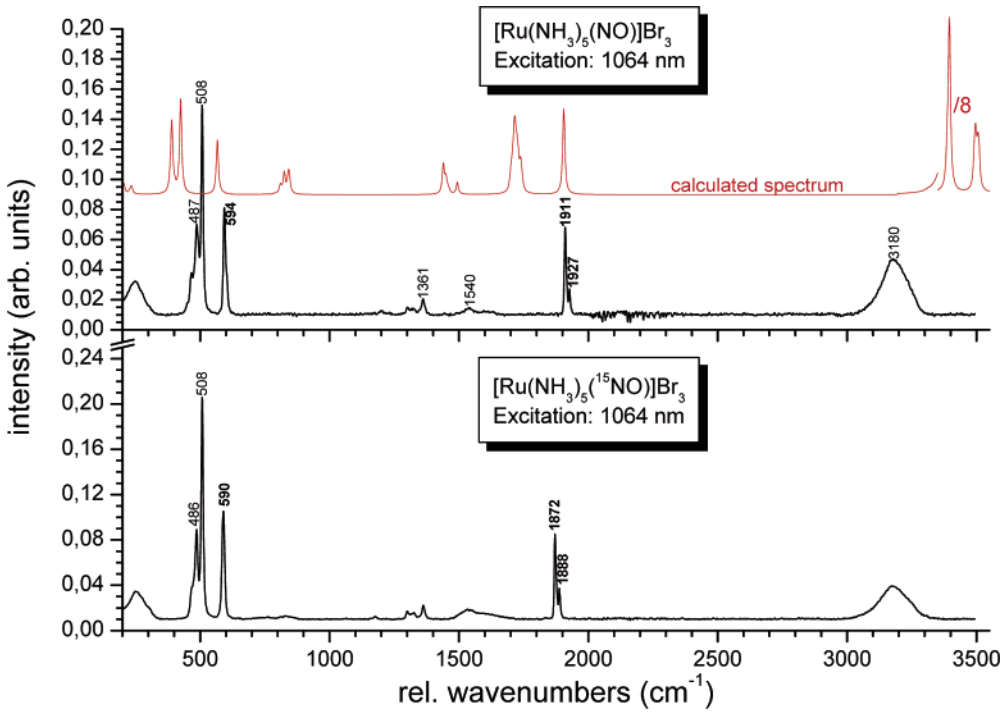

Figure 3. Raman spectrum of **2-Br** (top) and of the corresponding ^{15}N isotope labeled complex (bottom). The calculated spectrum is also included in the top panel as indicated.

intrinsic feature of the $[Ru(NH_3)_5(NO)]^{3+}$ cation but is related to the crystal structure of the bromide salt.

A.3. Normal Coordinate Analysis (NCA). The assignments of the vibrations of the $[Ru(NO)]^{3+}$ subunit presented above are confirmed by NCA using model $\hat{2}$. As shown in Table 2, excellent agreement is obtained between the experimental and NCA frequencies when ^{15}NO is used as the isotopically labeled ligand. The expected isotope shifts for $^{15}N^{18}O$ are also shown. Strikingly, these are about twice as large as the shifts observed spectroscopically. This proves that the ^{18}O in the applied $^{15}N^{18}O$ gas was exchanged against an unlabeled oxygen during synthesis yielding the corresponding ^{15}NO complex (see Discussion section). In addition, the calculated ^{15}N isotope shifts clearly show that the assignment of the 594 cm^{-1} Raman band to ν(Ru−NO) (isotope shift: 4 cm^{-1}) and of the 602 cm^{-1} IR band to

Table 2. Comparison of Experimental and QCA-NCA Vibrational Frequencies [cm^{-1}] and of QCA-NCA and Calculated (DFT) Force Constants [mdyn/Å] for $[Ru(NH_3)_5(NO)]Br_3$ (**2-Br**)

	exptl		QCA-NCA			force constant, *f*	
mode	nai[a]	^{15}NO	nai[a]	^{15}NO	($^{15}N^{18}O$)	QCA-NCA	calcd[b]
ν(N−O)	(1927)/1911	(1888)/1872	1911	1872	(1829)	15.338	15.357
ν(Ru−NO)	594	590	594	589	(574)	5.041	4.644
δ(Ru−N−O)	602	588	603	587	(583)	0.664	0.646

[a] nai = natural abundance isotopes. [b] Calculated with B3LYP/LanL2DZ; see Experimental Section. Free NO: ν(N−O) = 1876 cm^{-1}; f_{N-O} = 15.49 mdyn/Å. NO^+: ν(N−O) = 2387 cm^{-1} in $(NO^+)(BF_4^-)$; f_{N-O} = 25.07 mdyn/Å.[34]

Table 3. Comparison of Experimental and Calculated Bond Distances [Å]

	Δ(Ru−NO)	Δ(N−O)	Δ(Ru−NH_3), trans	Δ(Ru−NH_3), cis
2-Br, cryst struct	1.913[a]	1.019	2.087[b]	2.096[b]
$[Ru(NH_3)_5(NO)]^{3+}$	1.802	1.166	2.175	2.199[b]

[a] Overestimated since the experimental bond distance is actually an average of a Ru−NO and a Ru−NH_3 bond length due to the observed disorder in the crystal. [b] Averaged over all corresponding bond lengths.

δ(Ru−N−O) (isotope shift: 14 cm^{-1}) as presented above is correct. These shifts are well reproduced by the NCA as shown in Table 2. Force constants are discussed in the next section.

A.4. Electronic Structure and Spectra. Figure 1B shows the fully optimized structure of the $[Ru(NH_3)_5(NO)]^{3+}$ cation. Important bond lengths are compared to experiment in Table 3. Unfortunately, due to the disorder in the crystal (vide supra), the most interesting comparison between the experimental and the calculated Ru−NO distance is obscured. Other distances are in reasonable agreement. A more sophisticated comparison is available from the experimental and calculated force constants and vibrational frequencies given in Table 2. In the calculation, the Ru−NO and even more the Ru−NH_3 frequencies are obtained at too low an energy indicating that the metal−ligand bond strengths are generally underestimated in the calculation. This can also be seen from the Ru−NO force constant, which is calculated to 4.64 mdyn/Å compared to the experimental value of 5.04 mdyn/Å. The obtained bonding description is analyzed in the following.

The MO diagram of the free NO molecule is shown in Figure 5 in the Supporting Information. Free NO is a radical with the unpaired electron occupying one of the π^* orbitals. Due to the short NO bond distance, the energy difference between the singly occupied π^* orbital and the next lower occupied orbital σ_{nb} is quite large. The orbital σ_{nb} is a combination of sp hybrids along the N−O axis but is only weakly N−O bonding. Just below σ_{nb}, the two N−O π orbitals are located. The complex $[Ru(NH_3)_5(NO)]^{3+}$, formally a $Ru^{3+}-NO^{\bullet}$ adduct, actually has an electronic structure corresponding to $Ru^{2+}-NO^+$. This is evident from the linear Ru−N−O unit and the observed N−O stretching frequency of >1900 cm^{-1} as described in the literature.[29,5e] This is also reflected by the obtained MO diagram of $\tilde{\mathbf{2}}$ given in Figure 6 in the Supporting Information. Figure 1b shows the coordinate system used in the following discussion with the Ru−N−O unit located on the *z* axis. Since NO is bound as NO^+, its π^* orbitals are both empty and form a back-bond with the two t_{2g} orbitals d_{xz} and d_{yz} of Ru. The corresponding antibonding combinations, $\pi^*\_d_{xz}$ and $\pi^*\_d_{yz}$, are the LUMO of complex **2**. They have about 70% π^* and 25% d character, which corresponds to strong back-bonding. The corresponding bonding combinations, $d_{xz}\_\pi^*$ and $d_{yz}\_\pi^*$, are occupied and have 68% d and 26% π^* contribution. The third t_{2g} orbital, d_{xy}, is also occupied and corresponds to the HOMO of **2**. This shows that Ru is in the +2 oxidation state and low-spin in agreement with the $Ru^{2+}-NO^+$ description. The strength of the π back-bond is reflected by the N−O force constant of 15.34 mdyn/Å, which is distinctively lower than that of NO^+ and actually is very close to that of free NO.[34] Hence, a large amount of electron density is transferred from Ru^{2+} to NO^+ through the π system. Besides these two strong π back-bonds, there is also a Ru−NO σ bond mediated by the orbital σ_{nb}. The bonding combination, $\sigma_{nb}\_d_{z^2}$, has 5% d_{z^2} contribution which corresponds to a weak interaction. This bonding description is also reflected by the calculated NPA charges and d orbital populations given in Table 4. The formal +1 charge of the NO^+ ligand is reduced

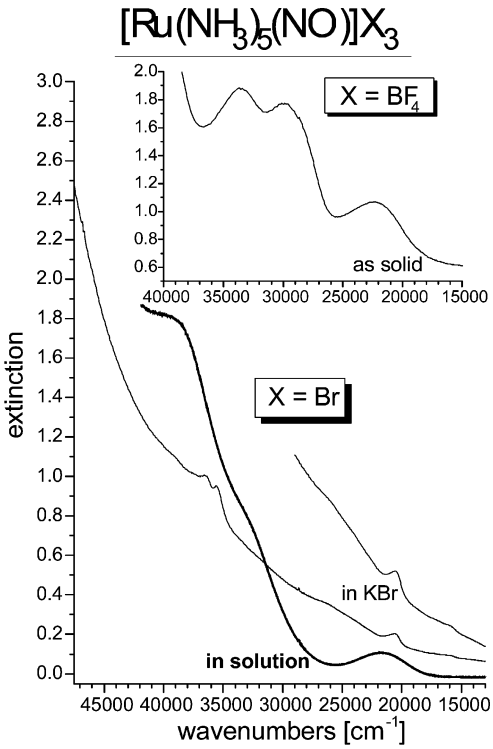

Figure 4. Low-temperature absorption spectra of $[Ru(NH_3)_5NO]Br_3$ as KBr disk and $[Ru(NH_3)_5NO](BF_4)_3$ (insert) as a solid measured between sapphire windows. For the bromide salt, a solution spectrum is also shown.

(34) Fadini, A.; Schnepel, F.-M. *Schwingungsspektroskopie*; Thieme Verlag: Stuttgart, 1985.

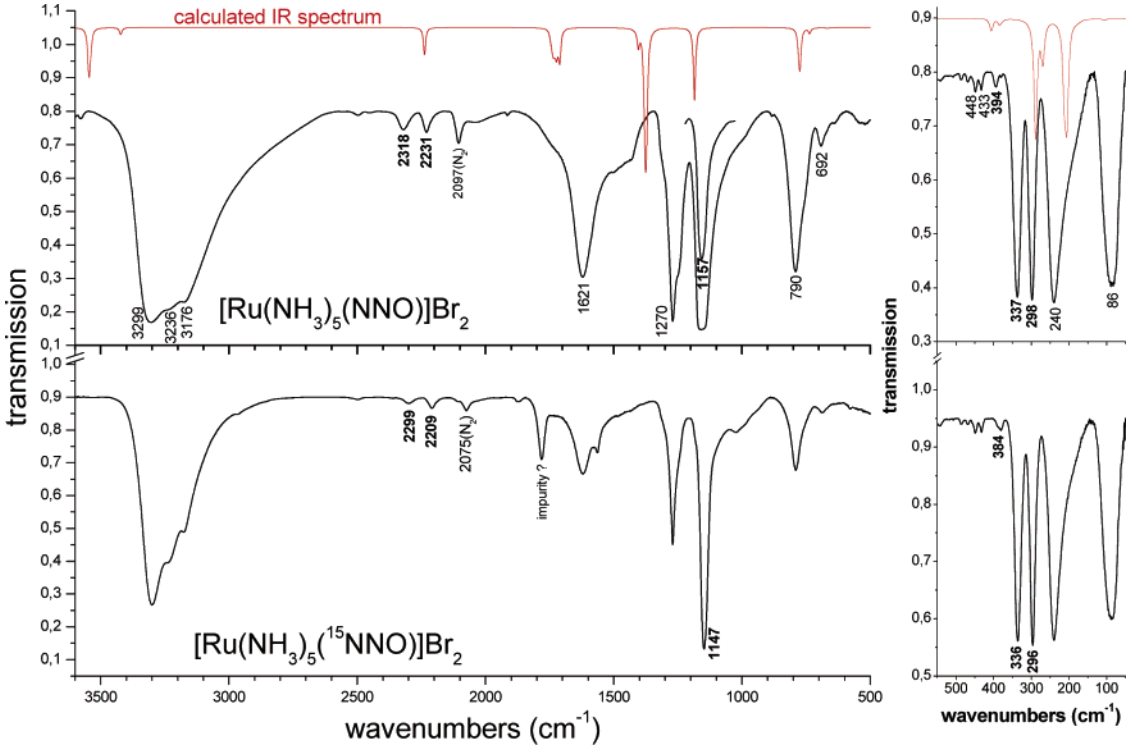

Figure 5. IR spectrum of **1-Br** (top) and of the corresponding ^{15}NNO isotope labeled complex (bottom). The calculated spectrum is also included in the top panel as indicated.

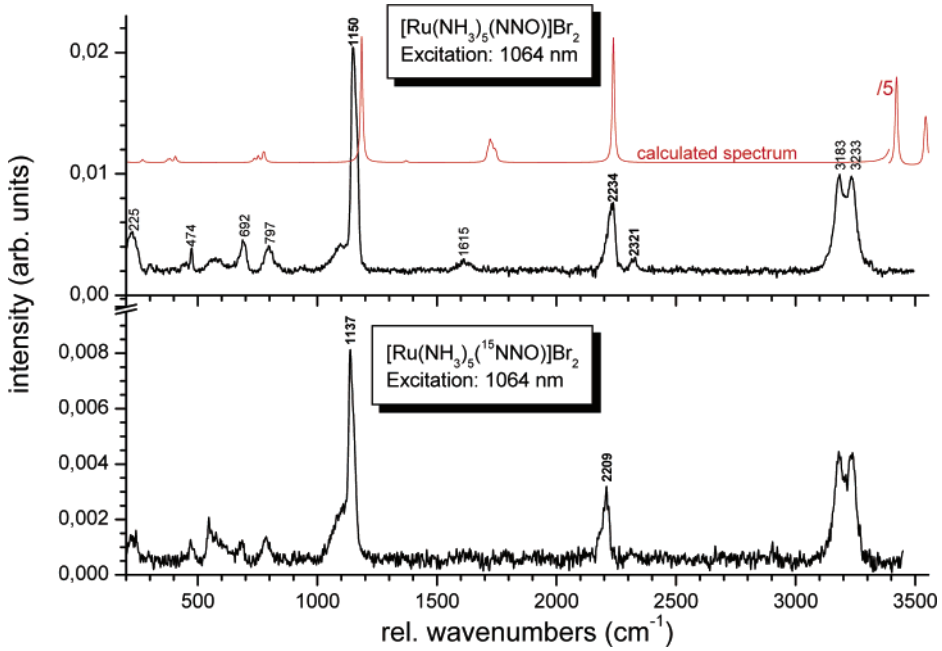

Figure 6. Raman spectrum of **1-Br** (top) and of the corresponding ^{15}NNO isotope labeled complex (bottom). The calculated spectrum is also included in the top panel as indicated.

Table 4. Calculated NPA Charges and d Orbital Populations of $[Ru(NH_3)_5(NO)]^{3+}$

NPA charges			NPA d orbital populations			
Ru	N	O	d_{xy}	d_{xz}	d_{yz}	$d_{z^2} + d_{x^2-y^2}$
+0.77	+0.35	+0.08	1.81	1.57	1.57	2.01

to +0.43 by back-donation from the d_{xz} and d_{yz} orbitals of Ru. Accordingly, their population is reduced to +1.57 compared to +1.81 for the nonbonding orbital d_{xy}. This roughly corresponds to a net transfer of half an electron from d_{xz} and d_{yz} to the NO^+ ligand in accordance with its NPA charge. The large occupation number for the e_g orbitals of 2.01 is due to the strong donation of the NH_3 ligands. Contour plots of important molecular orbitals are shown in Figure 7 in the Supporting Information.

With the help of the calculated electronic structure of $\tilde{\mathbf{2}}$ and a time-dependent (TD) DFT calculation, the electronic absorption spectra of complexes **2** can be assigned. Figure 4 shows the obtained data for **2-Br** (in a KBr disk and in

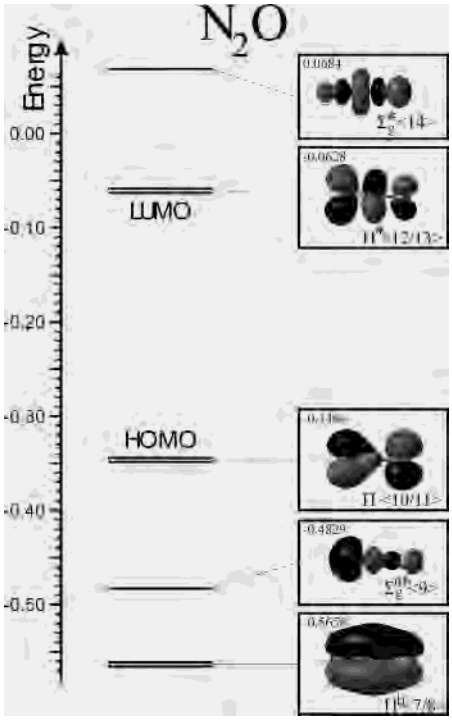

Figure 7. MO diagram of free N_2O and contour plots of important orbitals. Energies are given in Hartree.

Table 5. Experimental Absorption Band Positions [cm^{-1}] for $[Ru(NH_3)_5(NO)]X_3$ (**2**) and Assignments

assignment	TD-DFT	**2-Br** (X = Br)[a]		**2-BF$_4$** (X = BF_4)	**2-OTf** (X = OTf)[b]
$^1\Gamma \rightarrow {}^3\Gamma$[c]		15990			
$d_{xy} \rightarrow \pi^*\_d$	22222	20550	(21850)	22260	22940
$d_{xy} \rightarrow e_g$	28820			29450	
$d_{xy} \rightarrow e_g$	35840		(33170)	33765	33230
$d\_\pi^* \rightarrow e_g$	38680	35400 36490	(38470)		

[a] Solution data in brackets. [b] Data not shown. [c] Spin forbidden transition.

solution) and **2-BF$_4$** (as a solid). Importantly, no intense charge transfer transition is observed above 200 nm. According to the MO diagram of $\tilde{\mathbf{2}}$, the lowest energy charge transfer should correspond to a transition from the bonding (d_π^*) to the antibonding (π^*_d) MOs of the Ru−NO π bond. However, as discussed here, the splitting between these orbitals is large due to the strength of the back-bond. Hence, this transition should be at high energy below 200 nm and, accordingly, is not observed experimentally (cf. Figure 4). The observed weak absorptions are therefore assigned to d−d transitions as given in Table 5. Around 20000 cm^{-1}, the first (spin allowed) transition from d_{xy} to the antibonding orbitals π^*_d is observed. At higher energy, the transitions from d_{xy} to the e_g orbitals d_{z^2} and $d_{x^2-y^2}$ occur. These can be associated with the bands at 29450 and 33765 cm^{-1} in the solid state spectrum of **2-BF$_4$** and the band at 33230 cm^{-1} in **2-OTf**. In addition, the solution spectrum of **2-Br** shows a corresponding transition at 33170 cm^{-1}. Interestingly, these bands appear to be missing in the spectrum of **2-Br** measured in KBr. In this case, a split band at 36490 and 35400 cm^{-1} is observed that is tentatively assigned to the transitions from the $d_{xz}\_\pi^*$ and $d_{yz}\_\pi^*$ orbitals to e_g.

B. Spectroscopy and Electronic Structure of $[Ru(NH_3)_5(N_2O)]^{2+}$ (1). Vibrational data are presented for $[Ru(NH_3)_5(N_2O)]X_2$ (**1**) and analyzed with the help of DFT calculations and a normal coordinate analysis. From the calculations, the properties of N_2O as a ligand are determined, and the electronic structure of **1** is defined. In addition, DFT is used to calculate formation constants for different $[Ru(NH_3)_5(L)]^{2+}$ complexes. Finally, the potential reactivity of end-on terminally bound N_2O for N−O bond cleavage mediated by protonation and reduction is explored.

B.1. Vibrational Spectra and Assignments. The IR spectrum of $[Ru(NH_3)_5(N_2O)]Br_2$ is shown in Figure 5 together with the corresponding ^{15}NNO isotope labeled complex. As will be shown in section B.4, these data are only compatible with N_2O being end-on coordinated with the nitrogen atom. Hence, for the following analysis this bonding mode of nitrous oxide is used. In Figure 5, isotope sensitive bands are present at 2231 and 1157 cm^{-1} in the MIR region that shift to 2209 and 1147 cm^{-1} in the ^{15}NNO complex. These are assigned to the N−N stretch and the N−O stretch of the nitrous oxide ligand, respectively, in agreement with the literature.[3] An additional isotope sensitive band at 2318 cm^{-1} is assigned to the first overtone of the N−O stretch at 1157 cm^{-1}. The feature at 2097 cm^{-1} belongs to the corresponding $[Ru(NH_3)_5(N_2)]^{2+}$ complex that is found as an impurity in **1-Br**. It is observed at 2075 cm^{-1} in the corresponding ^{15}NN complex. Figure 6 shows the first Raman spectra recorded for an N_2O complex. The band positions of the N−N and N−O stretches at 2234 and 1150 cm^{-1}, respectively, are comparable to the IR results. Other isotope sensitive bands are found in the far-IR spectra in Figure 5. Intense bands at 338 and 298 cm^{-1} shift to 336 and 296 cm^{-1} in the ^{15}NNO complex. The band at 298 cm^{-1} is assigned to the Ru−NNO stretch, whereas the other feature corresponds to a N−Ru−N octahedral bend that is mixed with the Ru−N−N linear bend (vide infra).

Calculated IR and Raman spectra for $[Ru(NH_3)_5(NNO)]^{2+}$ are shown in Figures 5 and 6 in comparison with experimental results for **1-Br**. Table 6 summarizes the complete assignments. The positions of the N−H vibrations of the $[Ru(NH_3)_5]^{2+}$ subunit are somewhat changed compared to the Ru(II)−NO^+ complexes **2**, but the overall assignments of the $\nu_{as/s}$(N−H) stretches, the $\delta_{as/s}$(H−N−H) bends, and the δ(Ru−N−H) bends are very similar and can be extracted from Table 6. Calculated energies of ν(N−N) and ν(N−O) for $\tilde{\mathbf{1}}$ are in very good agreement with experiment. At lower energy, the linear bends δ(N−N−O) are calculated around 410 cm^{-1} with very low IR and Raman intensity. Correspondingly, these bands are not observed experimentally. On the other hand, the Ru−NH_3 stretching vibrations are calculated too low in energy as in the case of $[Ru(NH_3)_5(NO)]^{3+}$. Bands occurring at 474 cm^{-1} in the Raman spectrum and at 448 and 433 cm^{-1} in the IR data of **2-Br** can be associated with these modes.[35] To lower energy, two bands are observed at 338 and 298 cm^{-1} in the far-IR spectrum. The occurrence of two quite intense bands around 300 cm^{-1} is a signature of the Ru(II)−N_2O complex, since

Table 6. Vibrational Assignments of $[Ru(NH_3)_5(NNO)]X_2$ in Comparison to Results Obtained From DFT Calculations

		$[Ru(NH_3)_5(NNO)]^{2+}$ (calculated)[a]		$[Ru(NH_3)_5(NNO)]Br_2$		$[Ru(NH_3)_5(NNO)](BF_4)_2$	
number of modes	mode	frequency [cm^{-1}]	intensity	nai[b]	^{15}NNO	nai[b]	^{15}NNO
10	ν_{as}(N−H)	range: 3537−3548	s, IR/s, R	3299/3236(IR) 3233(R)		3371(IR) 3374(R)	
5	ν_s(N−H)	range: 3419−3425	vs, R/w, IR	3183(R) 3176(IR)		3302/3224(R) 3301(IR)	
1	ν(N−N)	2238	vs, R/s, IR	2234(R) 2231(IR)	2209(IR, R)	2269(R) 2270(IR)	2243(R) 2244(IR)
10	δ_{as}(H−N−H)	range: 1710−1748 1741/1735 1724/1710	w, R s, IR s, IR	1621(IR)/1615(R)		1636(IR)/1640(R)	
5	δ_s(H−N−H)	range: 1361−1404 1379/1374/1371	−, R vs, IR	1270(IR)		1297(IR)	
1	ν(N−O)	1185	vs, IR/vs, R	1150(R) 1157(IR)	1137(R) 1147(IR)	1197(R) 1206(IR)	1182(R) 1192(IR)
10	δ(Ru−N−H)	range: 619−779 779/775/773 738/736	 s, IR/w, R w, IR/w, R	 797(R)/790(IR) 692 (IR, R)		 770(IR) 755(R)	
2	δ(N−N−O)	408/406	−, IR/−, R	394 (IR)?	384(IR)?	454(IR)?	450(IR)?
5	ν(Ru−NH_3)	range: 373−406 406(A_1) 384	 w, R/w, IR w, IR	 474(R) 448/433 (IR)		 452/429(R) 431/378(IR)	
1	ν(Ru−NNO)	289	m, IR/−, R	297.8(IR)	296.4(IR)	303.8(IR)	299.6(IR)
2	δ(N−Ru−N)*	271/268	w, IR/w, R	337.5	335.7	315.1	313.1
7	δ(N−Ru−N)	range: 171−212 212/207/204 183	 m, IR w, R	 240(IR) 225(R)		 245(IR) 228(R)	

[a] For a given type of vibration, range gives the range of vibrational energies obtained in the calculation. Below the range value, vibrations with a certain amount of IR and/or Raman intensity are listed for comparison with experimental data (vs, very strong; s, strong; m, medium; w, weak; −, no intensity). A_1 identifies the totally symmetric vibration when applicable. [b] nai = natural abundance isotopes.

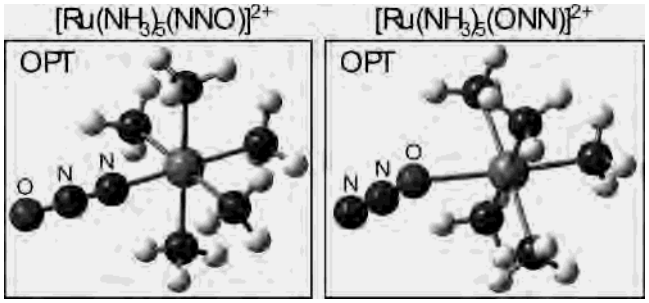

Figure 8. Fully optimized structures of the two coordination isomers of $[Ru(NH_3)_5(N_2O)]^{2+}$ (**1**). Note that the complex where nitrous oxide is bound end-on terminally through its nitrogen atom (on the left) corresponds to the experimental coordination mode (see section B.4). Structural parameters are given in Table 8.

they are absent in compounds **2** and other corresponding materials. They are also found for the tetrafluoroborate salt **1-BF_4** (see Supporting Information Figure 8). In this case, the two bands are close at 315 and 304 cm^{-1}. In the calculation, the Ru−NNO stretch is found at 288 cm^{-1}. Moreover, the calculation predicts two vibrations at 271 and 268 cm^{-1} that have predominant δ(N−Ru−N) character (labeled δ(N−Ru−N)*). These modes are shifted to higher energy compared to the remaining octahedral N−Ru−N bends by an admixture of the Ru−N−N linear bends which occur at much lower energy (<100 cm^{-1} in the calculation). Since both bands at 338 and 298 cm^{-1} in **1-Br** and the corresponding features at 315 and 304 cm^{-1} in **1-BF_4** are isotope sensitive, it is not straightforward which one of these corresponds to ν(Ru−NNO) and which to δ(N−Ru−N)*. However, since the δ(N−Ru−N)* modes also have some Ru−N−H bending character, they should be much more sensitive to a counterion change than the Ru−NNO stretch. Therefore, the bands at 338 cm^{-1} in **1-Br** and 315 cm^{-1} in **1-BF_4** are assigned to the octahedral bends δ(N−Ru−N)* and the features at 298 cm^{-1} in **1-Br** and 304 cm^{-1} in **1-BF_4** to ν(Ru−NNO). The fact that the δ(N−Ru−N)* vibrations occur at higher energy in experiment compared to the calculation is in agreement with the observed tendency for the remaining octahedral bends, which are observed around 240 cm^{-1} in the IR spectrum and calculated around 210 cm^{-1} (cf. Table 6). Table 6 also shows the assignments for the tetrafluoroborate salt **1-BF_4**, which are essentially identical

(35) Note that the ν(Ru−NH_3) vibrations of the Ru(II)−NO^+ complexes are much more intense in the Raman spectrum compared to their Ru(II)−NNO counterparts (compare the strong bands at 508 and 487 cm^{-1} of **2-Br** with the weak 474 cm^{-1} feature of **1-Br** in Figures 3 and 6). This is probably due to the decreased Ru−NH_3 bond strength and, hence, covalency in **1** compared to **2**.

Table 7. Comparison of Experimental and QCA-NCA Vibrational Frequencies [cm^{-1}] and of QCA-NCA and Calculated (DFT) Force Constants [mdyn/Å] for $[Ru(NH_3)_5(NNO)]Br_2$ (**1-Br**)

	exp. (cf. Table 6)		QCA-NCA		force constants	
mode	nai[a]	^{15}NNO	nai[a]	^{15}NNO	QCA-NCA	calcd[b]
ν(N−N)	2234	2209	2234	2209	17.270	17.591
ν(N−O)	1150	1137	1150	1136	9.603	9.732
ν(Ru−NNO)	297.8	296.4	297.6	296.3	1.435	1.486

[a] nai = natural abundance isotopes. [b] Calculated with B3LYP/LanL2DZ; see Experimental Section. Free N_2O: ν(N−N) = 2224 cm^{-1}; f_{N-N} = 17.88 mdyn/Å; ν(N−O) = 1286 cm^{-1}; f_{N-O} = 11.39 mdyn/Å.[36]

to **1-Br**. The corresponding IR and Raman spectra of **1-BF$_4$** are presented in the Supporting Information.

B.2. Normal Coordinate Analysis. The assignments of the vibrations of the $[Ru(NNO)]^{2+}$ subunit as already described are confirmed by NCA using model $\hat{\mathbf{1}}$. Due to the fact that the hydrogen atoms of the ammine ligands have been omitted in $\hat{\mathbf{1}}$, no accurate description of the δ(N−Ru−N)* vibrations is possible with the chosen model. Hence, the normal coordinate fit has been limited to the stretching modes of the $[Ru(NNO)]^{2+}$ subunit. As shown in Table 7, excellent agreement is obtained in these cases between the experimental and NCA frequencies. Importantly, the calculated force constants indicate a weakening of the N−O bond (free N_2O, 11.4 mdyn/Å; Ru−N_2O, 9.6 mdyn/Å) upon coordination of the N_2O ligand. In contrast, the N−N bond is only slightly affected (free N_2O, 17.9 mdyn/Å; Ru−N_2O, 17.3 mdyn/Å). The reasons for this finding are discussed in the next section. The calculated Ru−NNO force constant of only 1.4 mdyn/Å shows that nitrous oxide is a weak ligand.

B.3. Electronic Structure and Spectra. The MO diagram of free nitrous oxide is shown in Figure 7. In the following text, the bonding properties of this ligand are evaluated in comparison with N_2, which has been shown to be a moderately π back-bonding and weakly σ donating ligand.[37] The LUMO of N_2O is the degenerate set of fully antibonding π* orbitals, labeled $\Pi^*\langle 12/13\rangle$, as shown in the contour plot in Figure 7. Since these orbitals are somewhat lower in energy than the π* orbitals of N_2, nitrous oxide should be a back-bonding ligand comparable to or better than N_2. The HOMO of nitrous oxide, $\Pi\langle 10/11\rangle$, corresponds to the degenerate set of π orbitals that are practically nonbonding (cf. Figure 7). They are located at low energy which indicates that the π donor ability of N_2O should be limited. Next in energy is the weakly N−N and N−O σ bonding orbital $\Sigma_g^{nb}\langle 9\rangle$, which mostly has lone pair character on the terminal nitrogen. This orbital could therefore act as a σ donor. However, since this orbital is located at even lower energy than the corresponding σ orbital of N_2, the σ donor ability of N_2O should be weak. In summary, nitrous oxide can be expected to be a comparable π acceptor and a weaker σ donor than N_2.

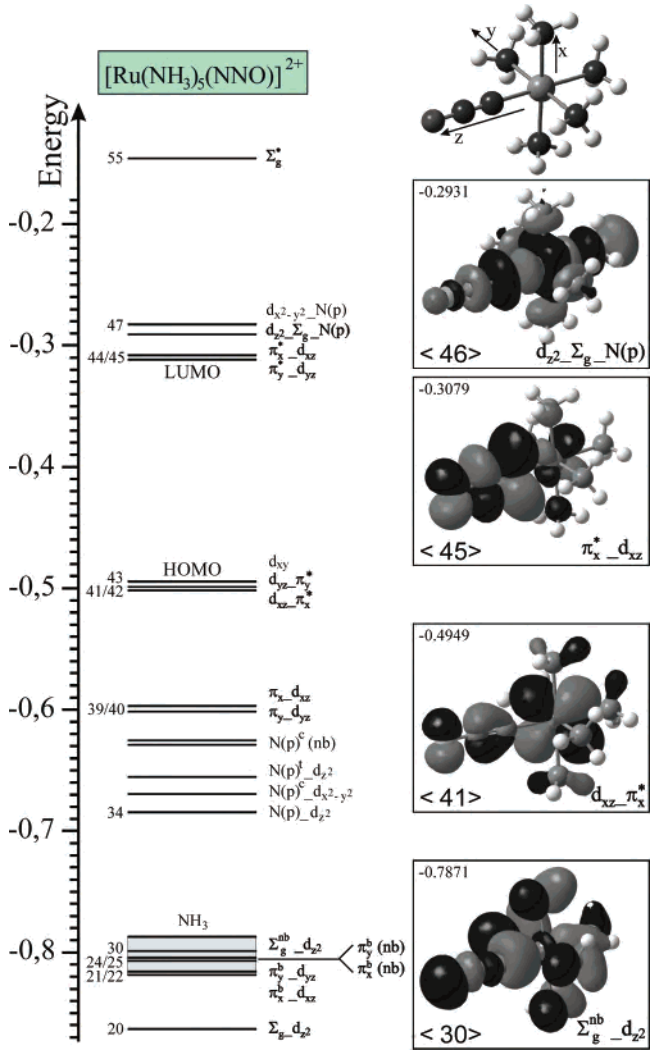

Figure 9. MO diagram of $[Ru(NH_3)_5(NNO)]^{2+}$ ($\tilde{\mathbf{1}}$) including contour plots of important molecular orbitals (right) and the applied coordinate system (top, right). Ligand orbitals of N_2O are labeled as given in Figure 7. The nomenclature "*a*_*b*" indicates that orbital *a* interacts with *b* and that *a* has a larger contribution to the resulting MO. Abbreviations: N(p) = lone-pair σ donor functions on the ammonia ligands; c = cis/t = trans with respect to N_2O; nb = nonbonding.

Figure 8, left, shows the optimized structure of $[Ru(NH_3)_5(NNO)]^{2+}$ ($\tilde{\mathbf{1}}$) where nitrous oxide is bound end-on through its terminal nitrogen atom. This leads to a linear coordination geometry with Ru−N−N and N−N−O angles close to 180°. As will be shown in section B.4, this is the experimental bonding mode of nitrous oxide in complex **1**, and hence, this bonding mode is applied here for the discussion of the electronic structure. Calculated bond lengths of $\tilde{\mathbf{1}}$ are presented in Table 8. For comparison, Figure 8 and Table 8 also include the coordination isomer of **1** where nitrous oxide is bound end-on through its terminal oxygen atom. This bonding mode is discussed in section B.4.

Figure 9 shows the MO diagram of $[Ru(NH_3)_5(NNO)]^{2+}$ ($\tilde{\mathbf{1}}$) and contour plots of important molecular orbitals. On the top, the optimized structure from DFT is shown together with the coordinate system that is used in the following discussion. In complex **1**, Ru is in the oxidation state +II and low-spin, which leads to a $[t_{2g}]^6$ electron configuration. Hence, since the t_{2g} orbitals (d_{xy}, d_{xz}, d_{yz}) are fully occupied,

(36) (a) Richardson, W. S.; Wilson, E. B., Jr. *J. Chem. Phys.* **1950**, *18*, 694. (b) Begun, G. M.; Fletcher, W. H. *J. Chem. Phys.* **1958**, *28*, 414−418.
(37) Lehnert, N.; Tuczek, F. *Inorg. Chem.* **1999**, *38*, 1671−1682.

Table 8. Comparison of Calculated Bond Distances [Å]

	Δ(Ru-L)	Δ(N−N)	Δ(N−O)	Δ(Ru−NH_3), trans	Δ(Ru−NH_3), cis
free N_2O (calcd)		1.161	1.241		
$[Ru(NH_3)_5(NNO)]^{2+}$ (**1̃**)	2.027	1.164	1.233	2.178	2.204[a]
$[Ru(NH_3)_5(ONN)]^{2+}$	2.294	1.153	1.262	2.151	2.206[a]

[a] Averaged over all corresponding bond lengths.

Table 9. Charge Contributions of Important Molecular Orbitals of $[Ru(NH_3)_5(NNO)]^{2+}$ (**1̃**)[a]

			Ru	N		N		O		ΣN[b]
no.	label	energy	d	s	p	s	p	s	p	s + p
⟨45⟩	π^*_x_d_{xz}	−0.3079	5	0	29	0	39	0	16	6
⟨44⟩	π^*_y_d_{yz}	−0.3087	5	0	28	0	39	0	16	7
⟨43⟩	d_{xy}	−0.4945	91	0	0	0	1	0	3	1
⟨42⟩	d_{yz}_π^*_y	−0.4947	82	0	1	0	4	0	9	1
⟨41⟩	d_{xz}_π^*_x	−0.4949	85	0	1	0	3	0	7	1
⟨40⟩	π_x_d_{xz}	−0.5984	6	0	34	0	0	0	47	12
⟨39⟩	π_y_d_{yz}	−0.5988	6	0	34	0	0	0	48	11
⟨30⟩	Σ_g^{nb}_d_{z^2}	−0.7871	2	6	14	1	11	10	11	32

[a] Additional MOs are given in Table 9 in the Supporting Information. [b] Contribution of the ammonia nitrogens.

no π donation from the N_2O ligand is possible in the linear Ru−NNO bonding mode of **1**. Accordingly, the observed orbital mixings between ligand orbitals Π and Π[b] and t_{2g} functions of Ru(II) do not contribute to bonding (cf. Figure 9 and Table 9). The HOMO of complex **1̃** is the d_{xy}⟨43⟩ orbital which is nonbonding. The other two t_{2g} orbitals of Ru(II), d_{xz} and d_{yz}, form a π back-bond with the unoccupied Π* orbitals of N_2O (the LUMO of the ligand). The corresponding bonding combinations, d_{xz}_π^*_x⟨41⟩ and d_{yz}_π^*_y⟨42⟩, are located very close in energy to the nonbonding d_{xy} orbital. This indicates that the Ru−NNO backbond is weak. The contour plot of d_{xz}_π^*_x⟨41⟩ (and correspondingly d_{yz}_π^*_y⟨42⟩) shows a very small coefficient on the coordinating nitrogen of the N_2O ligand. This is due to π/π^* mixing, i.e., mixing of these orbitals with Π⟨10/11⟩ of N_2O. The antibonding combinations, π^*_x_d_{xz}⟨45⟩ and π^*_y_d_{yz}⟨44⟩ are the LUMO of complex **1̃**. They have about 5% metal contribution which is in agreement with the weak π back-bond. Note that the occupied orbitals d_{xz}_π^*_x and d_{yz}_π^*_y are strongly N−O antibonding due to the π/π^* mixing already described, which explains the observed weakening of the N−O bond upon coordination of N_2O (vide supra). The Ru−NNO σ bond is mediated by the ligand orbital Σ_g^{nb} which interacts with d_{z^2}. However, the corresponding bonding combination, Σ_g^{nb}_d_{z^2}⟨30⟩, only has 2% metal contribution (cf. Table 9) which corresponds to a very weak interaction. In summary, this bonding description shows that the Ru−NNO bond is extremely weak in agreement with the experimental observation that the N_2O ligand in **1** is easily replaced with water and other ligands. This electronic structure is also in agreement with the calculated d orbital populations given in Table 10. Importantly, both backbonding orbitals d_{xz} and d_{yz} have about the same occupation number as the nonbonding orbital d_{xy}, which again indicates the weak back-bond in **1̃**. The large occupation of the e_g orbitals is due to the strong donation of the ammines (cf. Table 9 in the Supporting Information).

Table 10. Calculated NPA Charges and d Orbital Populations of $[Ru(NH_3)_5(NNO)]^{2+}$

NPA charges				NPA d orbital populations			
Ru	N	N	O	d_{xy}	d_{xz}	d_{yz}	$d_{z^2} + d_{x^2-y^2}$
+0.61	−0.16	+0.44	−0.22	1.95	1.90	1.90	1.42

Low-temperature absorption spectra of **1-Br** and **1-BF_4** are shown in Figure 10. In the case of **1-BF_4**, it was possible to obtain a solid state spectrum which allows for the identification of weak transitions (vide supra). Two bands are observed at 28875 and 36150 cm^{-1} (346 and 277 nm, respectively). From the MO diagram, the splitting of the three t_{2g} orbitals is marginal in complex **1** due to the weak backbonding capacity of nitrous oxide. Hence, the ligand field transitions can be assigned in first order using the Tanabe−Sugano diagram of low-spin d^6 systems. On the basis of this, the bands at 28875 and 36150 cm^{-1} are assigned to the $^1A_1 \rightarrow {}^1T_1$ and $^1A_1 \rightarrow {}^1T_2$ transitions, respectively. This is also in agreement with TD-DFT calculations. In addition, an intense charge transfer transition is observed in the KBr spectra of **1-Br** and **1-BF_4** (cf. Figure 10) around 42000 cm^{-1} (∼238 nm), which has also been observed in solution.[2] This band is characteristic for the Ru(II)−NNO unit since it is absent in the Ru(II)−NO^+ starting material (vide supra). This band is assigned to the d_π⟨41/42⟩ → π^*⟨44/45⟩ transition in agreement with TD−DFT calculations (predicted at 232 nm).

B.4. Binding Mode of Nitrous Oxide in 1. Two different binding modes for the nitrous oxide molecule in complex **1** have been discussed in the literature.[3,4] As shown in Figure 8, N_2O could potentially be bound end-on terminally to Ru(II) with either the nitrogen or oxygen atom. From the DFT calculations, these two binding modes lead to very different structures. When coordinated with the terminal nitrogen atom, the Ru(II)−NNO unit is linear, whereas binding with the oxygen atom leads to a strongly bent structure (the calculated Ru−ON(N) angle is 138°). However, due to the instability of complex **1**, no crystal structure could be determined. Hence, the bonding mode of nitrous oxide in **1** is uncertain. However, the mode of coordination can be determined from a correlation of the experimental data presented here for complex **1** with the results from the DFT calculations. On the basis of a normal coordinate analysis that was restricted to the four atoms of the Ru−N_2O subunit, it was claimed that the observed isotope shifts of the N−N and the N−O stretch are only in agreement with O coordination of N_2O.[3b,c] Contrary to these findings, Table 11 shows that the calculated isotope shifts for the N and O coordinated isomers of **1** (cf. Figure 8) are identical within a few wavenumbers and, hence, cannot distinguish between these isomers. Importantly, it is (a) the energy of the N−N and N−O stretches and (b) the far-IR spectral region that are actually most diagnostic for the mode of attachment of

Table 11. Comparison of Calculated Vibrational Energies and Isotope Shifts for N and O Coordinated Isomer of $[Ru(NH_3)_5(N_2O)]^{2+}$

	1-Br (exptl)		calcd $[Ru(NH_3)_5(NNO)]^{2+}$				calcd $[Ru(NH_3)_5(ONN)]^{2+}$			
mode	nai[a]	$^{15}N-N-O$	nai[a]	$^{15}N-N-O$	$N-^{15}N-O$	$N-N-^{18}O$	nai[a]	$O-N-^{15}N$	$O-^{15}N-N$	$^{18}O-N-N$
ν(N−N)	2234	−25	2238	−26	−46	−3	2160	−27	−43	−2
ν(N−O)	1150	−13	1185	−14	−3	−39	1091	−11	−3	−38
ν(Ru−X)	297.8	−1.4	289	−2	−2	−3	192	−1	−1	−5

[a] nai = natural abundance isotopes.

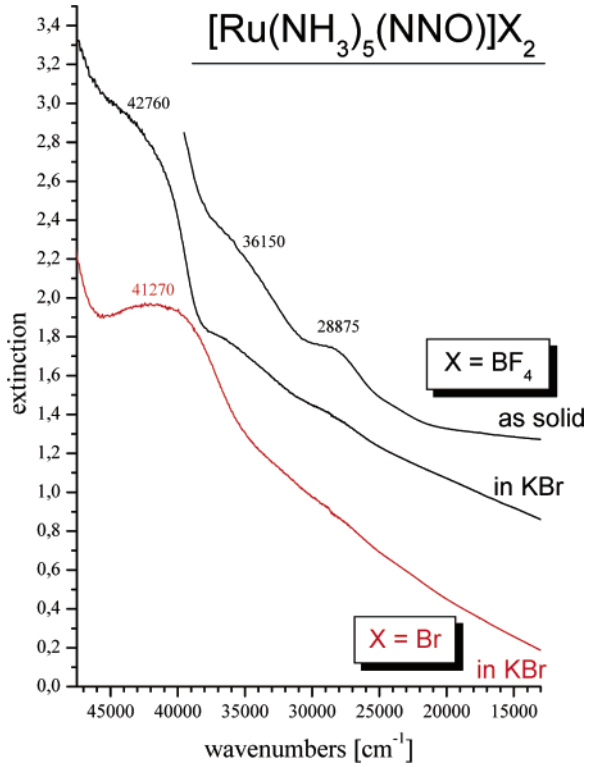

Figure 10. Low-temperature absorption spectra of $[Ru(NH_3)_5(NNO)]Br_2$ as KBr disk and $[Ru(NH_3)_5(NNO)](BF_4)_2$ in KBr and as a solid as indicated. Energies are given in cm^{-1}.

nitrous oxide. For ν(N−N) and ν(N−O), the calculated energy of the N bound isomer is close to the experimental value. In the far-IR region, the N coordinated isomer shows a pattern in the calculations with ν(Ru−N) occurring at ∼300 cm^{-1} (cf. Table 6) which is similar to experiment. In comparison, the Ru−ONN isomer has the corresponding ν(Ru−O) stretch below 200 cm^{-1} and no intense band in the 300 cm^{-1} region. Therefore, this clearly shows that the nitrous oxide ligand is N coordinated in compound **1**. The lower energy of the metal−ligand stretch in the O coordinated isomer reflects a weaker bound N_2O ligand in this case (the calculated Ru−O force constant is only 0.53 mdyn/Å). This is due to the fact that the Ru(II)−ONN isomer has a different electronic structure where no π back-bond or σ donor bond from Σ_g^{nb} is present. Instead, a pseudo-σ interaction between one of the Π orbitals (HOMO) of N_2O and d_{z^2} of Ru(II) is found which is extremely weak due to the low energy of Π (vide supra).

Due to the very different electronic structures of the O and N coordinated isomers of **1**, their calculated UV−vis absorption spectra are also very different. The calculated absorption spectrum for the N bound isomer (vide supra) shows the lowest energy ligand field transition around 400 nm and the intense charge transfer between the t_{2g} orbitals of Ru(II) and the nitrous oxide π^* orbitals around 230 nm. This is in very good agreement with experiment. On the other hand, for the O bound isomer, ligand field transitions are already predicted in the 540 nm region, and the intense $t_{2g} \rightarrow \pi^*$ transition is found around 350 nm. Hence, the experimental absorption spectrum also strongly favors N coordination of nitrous oxide in **1**.

Table 12. Reaction Energies for $[Ru(NH_3)_5]^{n+} + L \rightarrow [Ru(NH_3)_5(L)]^{n+}$ (T = 298.15 K) [kcal/mol]

complex	$\Delta\epsilon$[a]	ZPCE[a]	ΔH	ΔG	$\Delta\Delta G$	K_0[b]
$[Ru(NH_3)_5(NNO)]^{2+}$ (**1**)	−25.6	+1.4	−24.4	−14.1	0	
$[Ru(NH_3)_5(ONN)]^{2+}$	−16.9	+0.6	−16.2	−6.3	+7.9	
$[Ru(NH_3)_5(OH_2)]^{2+}$	−34.0	+2.4	−32.3	−22.4	−8.2	2×10^5
$[Ru(NH_3)_5(N_2)]^{2+}$	−31.8	+2.3	−30.3	−20.1	−6.0	5×10^3
$[Ru(NH_3)_5(NO)]^{3+}$ (**2**)	−62.4	+3.9	−59.6	−46.1		

[a] $\Delta\epsilon$: difference in electronic energy. ZPCE: zero point correction energy. [b] Equilibrium constant for the reaction $[Ru(NH_3)_5(NNO)]^{2+} + L \rightarrow [Ru(NH_3)_5(L)]^{2+} + N_2O$.

The relative stability of the N versus O coordinated isomer of **1** can also be investigated by total energy calculations of the ligand binding energy following the equation

$$[Ru(NH_3)_5]^{2+} + L \rightarrow [Ru(NH_3)_5(L)]^{2+} \qquad (2)$$

Table 12 shows the calculated ΔH and ΔG values for this reaction for L = NNO, ONN, N_2, and OH_2. Importantly, N coordination of nitrous oxide is more favorable than O coordination by 8 kcal/mol in terms of free energy. Comparing the stability of complex **1** (the N bound isomer) with corresponding N_2 and OH_2 complexes demonstrates the weakness of nitrous oxide as a ligand (vide supra). In fact, the N_2 and the OH_2 adducts are more stable than complex **1** by 6 and 8 kcal/mol in terms of free energy, respectively. This large difference in formation energy between the Ru(II)−N_2 adduct and the Ru(II)−NNO complex is rather surprising. The reasons for this finding are further evaluated in the Discussion section.

B.5. Reactivity of End-On Terminally N-Coordinated N_2O. Using DFT calculations, the reactivity of the Ru(II)−NNO complex toward protonation and reduction is explored in order to investigate the mechanism of the biologically relevant reaction of N_2O to N_2 and H_2O mediated by nitrous oxide reductase (see Introduction). As has been shown, nitrous oxide is a very weak ligand, and hence, activation toward protonation is hard to achieve. Scheme 1 shows two different reactions that were explored in this study. Initial protonation of $[Ru(NH_3)_5(NNO)]^{2+}$ ($\tilde{\mathbf{1}}$) leads to the formation of $[Ru(NH_3)_5(NN-OH)]^{3+}$ ($\tilde{\mathbf{1}}$ − H) with a bent N−O−H unit. The electronic structure of this intermediate is very

Scheme 1

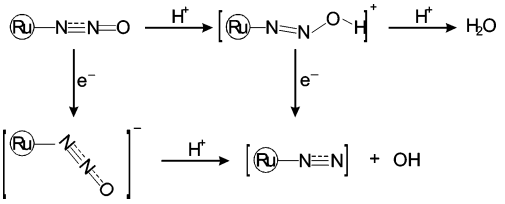

interesting. It has a distinctively weakened N−O bond with a force constant of only 4.76 mdyn/Å (compared to 9.73 mdyn/Å for $\tilde{\mathbf{1}}$), whereas the Ru−N bond is strengthened (force constant: 3.56 mdyn/Å compared to 1.49 mdyn/Å for $\tilde{\mathbf{1}}$). The reason for this finding is that the interaction of the proton 1s function with the Π_y and Σ_g^{nb} orbitals of N_2O leads to lowering of Π_y and Π_y* in energy and a mixing of these orbitals with σ orbitals like Σ_g^{nb}. In the case of Π_y*, this leads to a strong increase of mixing with d_{yz} which now has a 30% contribution to the resulting antibonding orbital, π_y^*_$d_{yz}\langle 44\rangle$ (the LUMO of $\tilde{\mathbf{1}}$ − **H**). This corresponds to a transfer of net electron density from the metal to the nitrous oxide ligand through the π back-bond and, hence, an oxidation of the metal upon protonation of the ligand. This electron transfer occurs smoothly through the π system which indicates that in general no barrier is to be expected for this process. The corresponding bonding combinations, d_{yz}_$\pi_y^*\langle 41\rangle$ and π_y_$d_{yz}\langle 35\rangle$, are N−O antibonding, which explains the weakening of the N−O bond upon protonation. The strengthening of the Ru−N bond, on the other hand, is due to the increased back-bond mentioned above and also due to a stronger interaction of Σ_g^{nb} with d_{z^2} in $\tilde{\mathbf{1}}$ − H. Contour plots of these important MOs are given in the Supporting Information. As shown in Scheme 1, a subsequent electron transfer to the Ru−NNOH intermediate leads to a splitting of the N−O bond and to the release of OH.[38] This is due to the fact that the additional electron occupies the π_y^*_$d_{yz}\langle 44\rangle$ orbital (the LUMO of $\tilde{\mathbf{1}}$ − H), which is strongly N−O antibonding.

The alternative mechanism where electron transfer precedes protonation is less favorable for two reasons. First, the transfer of one electron to $\tilde{\mathbf{1}}$ leads to the occupation of one of the π*_d_π antibonding orbitals. Since the Π* orbitals of N_2O are at high energy, this does not seem likely from a thermodynamic point of view; i.e., the required reduction potential can be expected to be too high for aqueous solutions. In addition, this breaks the already weak Ru−NNO back-bond, which forces the nitrous oxide ligand to rearrange to a bent structure as indicated in Scheme 1. In this case, the occupied Π* orbital now forms a pseudo-σ bond with the d_{z^2} function of Ru(II). This rearrangement is kinetically unfavorable and also bears the risk of losing the nitrous oxide ligand. In the reduced complex, the extra electron is mostly located on the N_2O ligand, which would therefore be highly activated for protonation. Nevertheless, because of the disadvantages described here, this mechanism can be excluded for the protonation and reduction of nitrous oxide.

(38) Note that the calculated release of the hydroxyl radical OH instead of OH^- after one electron reduction of $\tilde{\mathbf{1}}$ − **H** is due to the gas-phase nature of the calculations which disfavor charge separation.

The calculated free energy for the formation of $\tilde{\mathbf{1}}$ − **H** from $\tilde{\mathbf{1}}$ according to Scheme 1 is about +30 kcal/mol (including solvation effects in water). This shows that complex **1** is not able to perform this reaction in agreement with experiment. The reason for this is the low basicity of the coordinated nitrous oxide ligand in **1**, which is related to the weak Ru(II)−NNO back-bond (vide supra). Hence, the amount of charge transferred to the N_2O ligand upon binding to Ru(II) is too small to activate the ligand for protonation. This, in turn, relates to the oxidation potential of Ru(II), which is too high to allow for a significant amount of charge transfer. Importantly, this indicates that the application of more redox active (low valent) metal centers than Ru(II) would lead to an increase of nitrous oxide activation. In summary, although complex **1** is not activated for the protonation and reduction of nitrous oxide, the theoretical study of the corresponding reaction pathways offers a great deal of information on how transition metals can mediate the degradation of nitrous oxide and what the potential reaction mechanism is.

Discussion

In this study, the spectroscopic properties and the electronic structure of the only nitrous oxide complex isolated so far, $[Ru(NH_3)_5(NNO)]X_2$ (**1**, X = Br^-, BF_4^-), have been defined in comparison to the $[Ru(NH_3)_5(NO)]X_3$ (**2**) precursor. For the bromide salt of the nitrosyl complex (**2-Br**), a new crystal structure is presented. In this structure, the NO molecule is disordered in two positions due to symmetry (space group: *Pnma*). Interestingly, **2-Br** is isostructural to the corresponding chloride salt.[39] Furthermore, the vibrational properties of complex **2** with different counterions are investigated using isotope substitution and density functional calculations. This way, a complete assignment of the vibrational spectra of **2** was obtained. From normal coordinate analysis, force constants have been determined to 15.34 mdyn/Å for the N−O and 5.04 mdyn/Å for the Ru−NO bond in **2-Br**. From the observed linear Ru−N−O unit in the crystal structure of **2-Br** and the occurrence of ν(N−O) in the 1900 cm^{-1} region, it is generally accepted that **2** has a Ru(II)−NO^+ electronic structure.[29,5e] This is also found in the DFT calculations. The strength of the Ru−NO bond is mostly due to a back-bond between two d_π orbitals of Ru(II) and the unoccupied set of π* orbitals of NO^+. The corresponding antibonding molecular orbitals, for example, have 70% π* and 25% d_π character. This leads to a net transfer of approximately half an electron from the metal to the ligand and explains the lowering of the N−O stretching frequency from 2390 cm^{-1} in free NO^+ to ∼1900 cm^{-1} in complex **2**. In comparison to this back-bond, the Ru−NO^+ σ interaction is weak. An important consequence of this electronic structure is the occurrence of a partial positive charge on the nitrosyl nitrogen (calculated: +0.35), which leads to an activation toward nucleophilic attack.[5] Accordingly, it was reported that $[Ru(NH_3)_5(NO)]^{3+}$ is in equilibrium with

(39) Bottomley, F. *J. Chem. Soc., Dalton Trans.* **1974**, 1600−1605.

$[Ru(NH_3)_5(NO_2)]^+$ in alkaline solution[40] but is unaffected by acid.[39] It was surprising to us that the reaction of $[Ru(NH_3)_6]^{3+}$ with $^{15}N^{18}O$ in acidic aqueous solution led to the corresponding $[Ru(NH_3)_5(^{15}NO)]^{3+}$ complex where oxygen is unlabeled. On the other hand, dissolving the obtained $[Ru(NH_3)_5(^{15}NO)]^{3+}$ in ^{18}O labeled water (in neutral or acidic solution) did not lead to the incorporation of the labeled oxygen into the complex. Therefore, complex **2** is inert under these conditions. This means that the exchange of the ^{18}O label in the $^{15}N^{18}O$ gas must occur during the synthesis of **2**, i.e., during the reaction of $[Ru(NH_3)_6]^{3+}$ with $^{15}N^{18}O$. A possible explanation would be that the first step of the reaction is actually an outer sphere electron transfer:

$$[Ru(NH_3)_6]^{3+} + {}^{15}N^{18}O \rightarrow [Ru(NH_3)_6]^{2+} + [{}^{15}N^{18}O]^+ \quad (3a)$$

The formed NO^+ is then able to exchange its oxygen with the unlabeled water before coordination to Ru(II) occurs:

$$[{}^{15}N^{18}O]^+ + OH_2 \rightarrow [{}^{15}NO]^+ + {}^{18}OH_2 \quad (3b)$$

$$[Ru(NH_3)_6]^{2+} + [{}^{15}NO]^+ \rightarrow [Ru(NH_3)_5(^{15}NO)]^{3+} + NH_3 \quad (3c)$$

The electrophilic behavior of NO in complex **2** is used for the synthesis of the nitrous oxide complex $[Ru(NH_3)_5(N_2O)]X_2$ (**1**).[5b] In $[Ru(NH_3)_5(N_2O)]^{2+}$, possible coordination modes for the N_2O ligand are end-on terminally with either the nitrogen or oxygen atom. Since no crystal structure is available for this complex, the binding mode of N_2O to the Ru(II) center is uncertain.[41] However, a detailed analysis of the vibrational properties and of the electronic spectra connected to DFT calculations enabled us to unequivocally determine the bonding mode of N_2O in complex **1**. From these analyses, nitrous oxide is coordinated end-on terminally through its N atom in complex **1**, which can therefore be formulated as $[Ru(NH_3)_5(NNO)]^{2+}$. From NCA, force constants are determined to be 17.27, 9.60, and 1.44 mdyn/Å for the N−N, N−O, and Ru−NNO bonds, respectively. Compared to free nitrous oxide,[36] the N−N force constant is almost unchanged upon coordination whereas the N−O force constant of 11.39 mdyn/Å is distinctively lowered. Hence, the N−O bond is weakened upon coordination of the N_2O ligand. Low-temperature absorption spectra have also been recorded and completely assigned for **1**.

Experimentally, it was found that complex **1** easily loses nitrous oxide in solution, which indicates that N_2O is a weak ligand. This aspect is further investigated with the help of electronic structure calculations. Compared to dinitrogen, nitrous oxide is a comparable π acceptor (mediated by its degenerate π^* LUMO), but an even weaker σ donor, because the corresponding Σ_g^{nb} orbital of N_2O is at lower energy. Altogether, one would expect that the complex stability of $[Ru(NH_3)_5(NNO)]^{2+}$ is comparable to $[Ru(NH_3)_5(NN)]^{2+}$. This is not the case: experimentally, it was found that the reaction

$$[Ru(NH_3)_5(NNO)]^{2+} + N_2 \rightarrow [Ru(NH_3)_5(N_2)]^{2+} + N_2O$$

is exothermic is terms of free energy by −5.6 kcal/mol.[2a] This value compares well with the calculated ΔG of −6.0 kcal/mol. In addition, this is also in agreement with kinetically determined complex formation constants of a Ru(II) precursor (with an amine/phosphine ligand set) with dinitrogen and nitrous oxide.[6] The obtained data showed that the ratio of complex formation constants $K(N_2)/K(N_2O)$ is approximately 10^3, which is in good agreement with the calculated value of 5×10^3 (cf. Table 12) in favor of the N_2 complex. The reason for the reduced complex stability of the Ru(II)−NNO adduct is that nitrous oxide has an additional set of occupied π donor orbitals (the HOMO). Since Ru(II) has a low-spin $[t_{2g}]^6$ configuration, no π donation into the t_{2g} functions is possible in the linear Ru−NNO geometry. Instead, this interaction is energetically unfavorable due to Coloumb repulsion which lowers the stability of the complex. Hence, nitrous oxide is an even weaker ligand than dinitrogen. The properties of the Ru−NNO bond in **1** can further be analyzed by comparison to Ru(II)−NO^+ complex **2**. The back-bond between the π^* orbitals of N_2O and d_π of Ru(II) is weak. This is evident from the corresponding antibonding combinations, $\pi^*\_d_\pi$, which only have about 5% metal contribution compared to 25% in the case of the nitrosyl complex. This accounts for the observed large difference in metal−ligand force constants between Ru−NO (5.04 mdyn/Å) and Ru−NNO (1.44 mdyn/Å). Note that the electronic structure of **1** has been investigated before; however, the calculations were of extended Hückel type which does not allow one to analyze binding energies, vibrational frequencies, or transition energies or to quantitatively evaluate the metal−ligand covalencies.[41] In that study, the authors concluded that the Ru(II)−NNO bond is dominated by σ interaction. However, this is not in agreement with the calculations presented here which indicate that the π back-bond is more important than the very weak σ interaction.

From the electronic structure description of **1**, it becomes clear that it is difficult to synthesize more stable nitrous oxide complexes. Since N_2O is a weak σ and π donor, a more stable metal−NNO bond must be achieved by increasing π back-bonding. In order to strengthen this interaction, the metal should be low valent with a $[t_{2g}]^6$ electron configuration. However, there would still be the problem that the occupied t_{2g} orbitals would have the unfavorable Coulomb repulsion with the π donor orbitals of N_2O. Hence, it is unclear if this approach would lead to more stable metal−N_2O complexes. This still needs to be explored experimentally. In the enzyme nitrous oxide reductase, on the other hand, nitrous oxide is bound to the fully reduced Cu_Z cluster (see Introduction). In this case, all copper ions are in the oxidation state +1, which corresponds to a d^{10} electron configuration. Since all the d-orbitals are fully occupied, bonding of nitrous oxide to the cluster must solely be due to back-bonding. In order to explore the mechanism for N_2O degradation in the end-on terminal coordination mode, we applied DFT calculations on the model $[Ru(NH_3)_5(NNO)]^{2+}$.

(40) Bottomley, F.; Crawford, J. R. *J. Chem. Soc., Dalton Trans.* **1972**, 2145.
(41) Tuan, D. F.-T.; Hoffmann, R. *Inorg. Chem.* **1985**, *24*, 871−876.

These results provide key information on how the protonation and reduction of nitrous oxide work on a molecular level. Importantly, the nitrous oxide ligand is activated for protonation by back-donation from the metal(s). Since back-donation is weak in the case of Ru(II), complex **1** is not able to undergo this reaction experimentally. However, in the case of Cu(I), the back-bond and, hence, the activation of N_2O can be expected to be much stronger. This is especially true for the side-on coordination mode of N_2O to Cu_Z favored by Ghosh et al. in their DFT study, where two metal centers simultaneously donate electron density to the ligand.[13] Initial protonation of the coordinated nitrous oxide automatically triggers the transfer of electron density from the metal(s) to the NNOH unit. Since the electron transfer occurs through the metal−NNOH π system, this process can be expected to be barrierless. If the reduction potential of the metal(s) is strong enough to transfer a large amount of electron density, this leads to a distinct weakening of the N−O bond which nicely prepares for N−O cleavage. Hence, this process can be classified as a proton transfer with concerted electron transfer (PT/ET). The following step of the mechanism is less clear, since it depends, for example, on the coordination mode of the NNOH intermediate. Either the second electron is transferred first leading to a splitting of the N−O bond and the formation of hydroxide, which is released and subsequently protonated in aqueous solution, or alternatively, the second proton could be transferred first which would then automatically trigger the transfer of the second electron (second PT/ET process). In any case, nitrous oxide is degraded this way yielding dinitrogen and water in a smooth and barrierless process.

Acknowledgment. This work was supported by the Deutsche Forschungsgemeinschaft (DFG; Grant LE 1393/1). Mrs. U. Cornelissen is acknowledged for recording the FT-Raman spectra of compounds **1** and **2**.

Supporting Information Available: IR and Raman spectra of **2-BF$_4$**, **2-OTf**, and **1-BF$_4$**. MO diagrams of free NO and of $\tilde{\mathbf{2}}$ as well as contour plots of important molecular orbitals of these species. MO contour plots for $\tilde{\mathbf{1}}$ − H. Details for the crystal structure determination of **2-Br** and tables of atomic coordinates, anisotropic displacement parameters, and geometric parameters. Complete vibrational assignments for **2**. Coordinates of the DFT fully optimized structures of $\tilde{\mathbf{1}}$ and $\tilde{\mathbf{2}}$. This material is available free of charge via the Internet at http://pubs.acs.org.

IC049302I